International Journal of Nanomedicine

Dovepress
Taylor & Francis Group

Open Access Full Text Article

ORIGINAL RESEARCH

Evaluation of Chitosan–Pimelate Buccal Film Loaded with Duloxetine-Modified Sage Lipid Carriers Nanoformulation for Effective Antidepressant Activity in a Rat Model

Walaa A El-Dakroury[1], Yousra A Nomier[2], Abdelrahman R Said[1], Magaji Garba Taura[3], Ahmed Soliman Doghish[4,5], Asem Shalaby[6], Omnia M Sarhan[1]

[1]Department of Pharmaceutics and Industrial Pharmacy, Faculty of Pharmacy, Badr University in Cairo (BUC), Badr City, Cairo, 11829, Egypt; [2]Pharmacology and Clinical Pharmacy Department, College of Medicine and Health Sciences, Sultan Qaboos University, Muscat, Oman; [3]Department of Anatomy, College of Medicine, University of Bisha, Bisha, 61922, Saudi Arabia; [4]Faculty of Pharmacy, Al-Azhar University, Nasr City, Cairo, 11651, Egypt; [5]Department of Biochemistry, Faculty of Pharmacy, Badr University in Cairo, Badr City, Cairo, 11829, Egypt; [6]Pathology Department, College of Medicine and Health Sciences, Sultan Qaboos University, Muscat, Oman

Correspondence: Walaa A El-Dakroury, Department of Pharmaceutics and Industrial Pharmacy, Faculty of Pharmacy, Badr University in Cairo (BUC), Badr City, Cairo, 11829, Egypt, Email walaa.ahmed2@buc.edu.eg; w_dakroury@yahoo.com; Yousra A Nomier, Pharmacology and Clinical Pharmacy Department, College of Medicine and Health Sciences, Sultan Qaboos University, Muscat, Oman, Email y.nomeir@squ.edu.om

---

Introduction: Chitosan-pimelate (CS-Pim) mucoadhesive buccal films were developed to improve the therapeutic efficacy of duloxetine (DLX) using sage oil-based lipid carriers (DLX-SLCs). This buccal nanoplatform addresses DLX's limited oral bioavailability and extensive first-pass metabolism by providing a non-invasive route with enhanced mucosal permeability and sustained release.

Methods: DLX-SLCs were optimized and characterized for particle size, zeta potential, and entrapment efficiency. The carriers incorporated into CS-Pim buccal films, which were evaluated for physicochemical properties, morphology, hydrophilicity, and mucoadhesive strength. In vivo antidepressant efficacy was assessed in a lipopolysaccharide (LPS)-induced rat depression model using behavioral tests, biochemical markers, and histopathological analysis.

Results: Optimized DLX-SLCs yielded an average size of 130.9±2.4 nm, zeta potential of −28.4 ±2.3 mV, and entrapment efficiency of 79.9 ± 3.8%. The selected film exhibited desirable physicochemical attributes, including uniform thickness, pH (7.08 ± 0.03), drug content (99.1 ± 0.4%), tensile strength (10.07 ± 0.34 N/cm^2), elongation at break (109.9 ± 7.3%), swelling index (124%), mucoadhesive strength (48.9 ± 2.38 g), and smooth surface via SEM. FTIR and DSC confirmed successful polymer modification, drug encapsulation, and amorphous dispersion of DLX within the matrix. Contact angle analysis confirmed improved hydrophilicity. DLX-SLCs buccal films exhibited superior curative efficacy compared to pure-DLX and the marketed-DLX in lipopolysaccharide (LPS)-induced rat depression model. Behavioral assessments demonstrated a 60% reduction in immobility time, an increase in open-arm entries, and sucrose preference by a 3.29-fold and 2-fold, respectively, compared to the LPS group. Biochemical analyses revealed reduced TNF-α, IL-1β, and cortisol levels by 67.6%, 64.4%, and 53%, respectively. Alongside increased serotonin and GABA levels by 1.64-fold and 3.5-fold, respectively. Histopathological findings confirmed significant neuroprotective effects.

Conclusion: DLX-SLCs incorporated into CS-Pim buccal films provide enhanced antidepressant efficacy and neuroprotective benefits, representing a bioadhesive and patient-compliant alternative to conventional DLX formulations for depression treatment.

Keywords: antidepressant, buccal, chitosan, duloxetine, mucoadhesion, pimelic acid

---

https://doi.org/10.2147/IJN.S569862
Received: 11 October 2025
Accepted: 23 January 2026
Published: 29 January 2026

Graphical Abstract

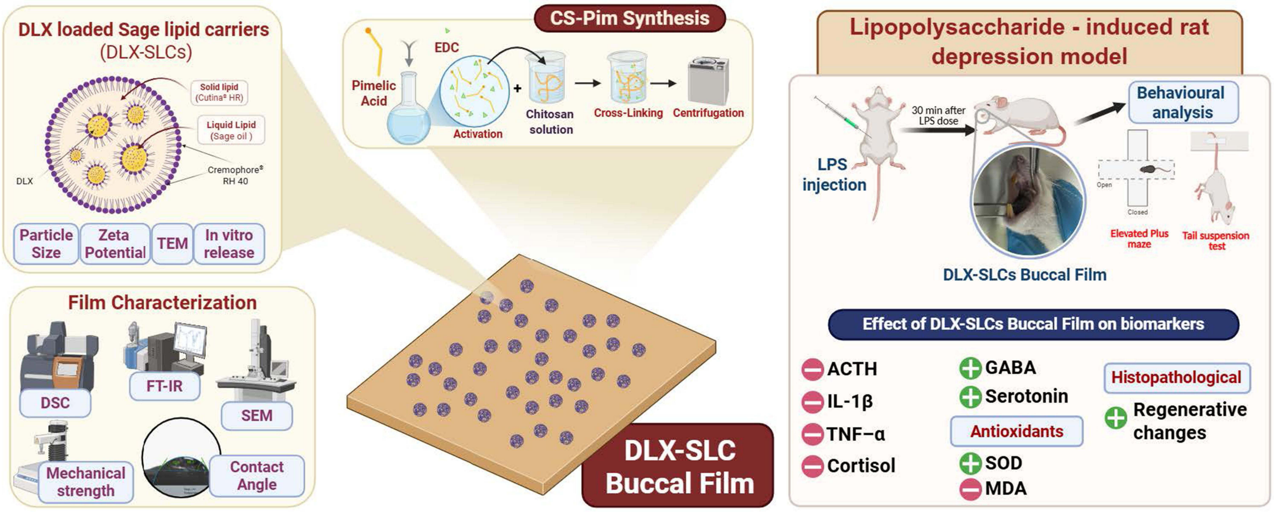

Introduction

Depression represents a significant global mental health concern, characterized by profound detrimental effects on both psychological well-being and physiological functioning. Current epidemiological data indicate that this disorder impacts approximately 264 million individuals worldwide and is associated with nearly 60% of global suicide-related mortality.[1] First-line pharmacological interventions, including first-generation tricyclic antidepressants (TCAs) and second-generation agents such as selective serotonin reuptake inhibitors (SSRIs), dopamine reuptake inhibitors (DRIs), and norepinephrine reuptake inhibitors (NRIs), remain the cornerstone of clinical management.[2] However, these therapeutic approaches are frequently limited by suboptimal efficacy, variable patient tolerance, and adverse side effects, which may compromise treatment adherence and long-term outcomes.[3] Consequently, there is an urgent need to advance the development of novel, safer, and more effective pharmacotherapeutic strategies to address the multifaceted challenges of depression management and improve patient quality of life.

Duloxetine (DLX), a second-generation antidepressant classified as a serotonin-norepinephrine reuptake inhibitor (SNRI), is widely prescribed as a first-line pharmacotherapy for major depressive disorder. Its therapeutic mechanism involves dual inhibition of presynaptic serotonin (5-HT) and norepinephrine (NE) transporters, thereby enhancing extracellular concentrations of these monoamines to ameliorate depressive symptomatology.[4] Compared to conventional antidepressants, such as tricyclic antidepressants (eg, amitriptyline, clomipramine, doxepin) and selective serotonin reuptake inhibitors (eg, citalopram), DLX demonstrates a distinct pharmacodynamic profile characterized by balanced monoaminergic reuptake inhibition, enhanced therapeutic efficacy, and improved tolerability.[3] Clinical evidence highlights its advantages, including a favorable safety profile, accelerated symptom remission, reduced adverse effects (eg, anticholinergic or cardiotoxic reactions), and minimal off-target receptor binding, collectively enhancing treatment adherence and patient outcomes.[5] These attributes underscore DLX's clinical utility in depression management.

DLX, despite exhibiting favorable oral absorption kinetics, demonstrates suboptimal systemic bioavailability (approximately 40%) owing to presystemic degradation in the acidic gastrointestinal environment and extensive first-pass metabolism mediated by hepatic cytochrome P450 1A2 (CYP1A2), reducing its therapeutic effectiveness and leading to variable patient responses.[4]

Lipid carriers (LCs) have emerged as a promising nanoplatform for enhancing the delivery of lipophilic drugs like DLX. LCs demonstrated significant efficacy in improving drug solubility and bioavailability, offering distinct advantages in stability, controlled release kinetics, and biocompatibility.[6] These LC systems are typically formulated using a matrix comprising biocompatible solid lipids classified as generally recognized as safe (GRAS) for oral, topical, and parenteral administration. Liquid lipids are often incorporated into the solid lipid matrix to optimize drug loading and release properties, creating a hybrid architecture combining both phases' benefits.[7]

Incorporating natural oils, such as sage oil, into LC formulations (SLCs) may further enhance their therapeutic potential. Sage oil possesses antioxidant and anti-inflammatory properties, which could synergistically augment the antidepressant effects of DLX.[8] In acute preclinical studies, linalool, a primary constituent of the essential oil derived from Salvia species (sage), has demonstrated potential antidepressant-like effects.[9] Emerging evidence suggests that its pharmacological activity may be mediated by the modulation of monoaminergic pathways, particularly through agonist-like interactions at serotonin 5-HT1A receptors and α2-adrenergic receptors.[10] These receptor systems are critically implicated in mood regulation, and their activation aligns with proposed mechanisms underlying linalool's acute neurobehavioral effects. Such findings highlight its potential as a phytochemical candidate for further investigation in depression-related therapeutics, though rigorous clinical validation remains necessary to elucidate its translational relevance.[11]

The therapeutic efficacy of antidepressants is contingent upon sustained drug concentration at the central nervous system (CNS) target site, particularly the brain. However, the blood-brain barrier (BBB), a highly selective interface characterized by tight endothelial junctions, efflux transporters (eg, P-glycoprotein), and metabolic enzymes, restricts systemic access to many orally administered antidepressants.[12] This limitation necessitates higher doses to achieve therapeutic CNS levels, increasing the risk of systemic adverse effects. Targeted drug delivery strategies that enhance BBB permeability or bypass systemic circulation can elevate cerebrospinal fluid (CSF) drug concentrations, enabling lower therapeutic doses while minimizing off-target toxicity. By optimizing brain-specific delivery, such approaches mitigate dose-dependent side effects and improve treatment adherence, underscoring the importance of advanced CNS-targeted formulations in depression management.[13]

As a BCS class-II agent characterized by low aqueous solubility and high membrane permeability, DLX presents a compelling candidate for alternative delivery strategies, such as buccal administration. Its physicochemical attributes, including moderate lipophilicity (log P = 4.2), molecular weight of 330 g/mol, and inherent permeability, align with the prerequisites for effective transmucosal drug delivery.[14] The buccal route offers potential advantages in bypassing hepatic metabolism and gastric degradation, enhancing efficiency and optimizing therapeutic outcomes. These properties position DLX as a viable candidate for innovative formulation approaches to overcome limitations.

Mucoadhesive buccal films can facilitate the buccal administration of DLX-loaded SLCs. Buccal drug delivery offers several benefits, including bypassing the hepatic first-pass effect, providing a rapid onset of action, and improving patient compliance due to its non-invasive nature.[15,16] Chitosan, a natural polysaccharide, is widely recognized for its mucoadhesive properties and biocompatibility, making it an ideal candidate for buccal film formulations.[17–19] However, native chitosan's limited solubility at physiological pH can hinder its effectiveness in buccal applications.[20] These constraints have prompted the development of novel chitosan derivatives engineered to enhance solubility across a broader pH range while improving mucoadhesive and permeation properties. Such derivatives are tailored to specific administration routes and dosage forms, with recent advancements focusing on structural modifications of free amine groups, thereby optimizing mucoadhesive performance.[21]

For instance, chitosan derivatives conjugated with fatty acids, including myristic, capric, azelaic, and stearic acids, have stabilized emulsion systems.[22] Studies indicate that increasing the carbon chain length of the fatty acid elevates polymer hydrophobicity, fostering robust interfacial network structures that improve emulsion stability compared to unmodified chitosan.[23] Furthermore, while native chitosan salts often exhibit rapid drug release, fatty acid-modified derivatives address this limitation by reducing polymer buccal solubility and delaying erosion, enabling prolonged and controlled drug release.[24,25]

For the first time, a novel chitosan derivative will be synthesized to enhance stability and mucoadhesive characteristics at buccal pH. One such derivative is chitosan pimelate, synthesized by conjugating chitosan with pimelic acid, a seven-carbon dicarboxylic acid. Pimelic acid's structure, comprising a hydrophobic hydrocarbon chain and a hydrophilic carboxylic acid group, coupled with its low aqueous solubility, enhances buccal pH stability.[26] This modification aims to improve the polymer's stability in the buccal environment and strengthen its interaction with the mucosal surface, thereby prolonging the residence time of the drug delivery system and enhancing drug absorption.

In this study, we propose developing a novel buccal film system comprising DLX-loaded SLCs incorporated into a chitosan pimelate matrix. This integrated approach seeks to leverage the benefits of SLCs for improved drug encapsulation and release, the therapeutic properties of sage oil, and the enhanced mucoadhesive performance of chitosan pimelate. The formulation aims to provide a sustained release of DLX, improved effectiveness, and enhanced anti-depressant efficacy, potentially offering a more effective treatment modality for patients with depression.

By integrating advanced nanotechnology with novel polymer chemistry, this research aims to develop an innovative buccal drug delivery system for DLX, potentially improving therapeutic outcomes for patients suffering from depression.

Materials and Methods

Cutina$^{®}$ HR powder was purchased from BASF, Germany. Chitosan (medium MWT) and pimelic acid were bought from Sigma-Aldrich (MO, USA). Duloxetine was gifted to us by EVA Pharmaceuticals (Cairo, Egypt). Sage oil was purchased from Harraz (Cairo, Egypt). Cremophor$^{®}$ RH 40 was gifted from Amoun Pharmaceuticals (Cairo, Egypt). Tween$^{®}$ 80 and glycerin were gifted from Sigma Quesna (Cairo, Egypt).

Preparation of Duloxetine Sage Lipid Carrier Nanoparticles

Sage lipid carrier (SLCs) nanoparticles were formulated via a hot homogenization and ultrasonication technique (Table 1).[27] Cutina HR, sage oil, and Cremophor RH 40 were combined in a 50 mL beaker and heated to 65°C until fully molten. DLX, 10 mg, was dissolved in the lipid phase, followed by adding 20 mL of an aqueous surfactant solution containing 100 mg of Tween 80, preheated to 65°C. The aqueous phase was introduced into the molten lipid under high-speed homogenization (12,000 rpm, 10 min; Homogenizer Model 302, Mechanika Precyzyjna, Warszawa, Poland) to generate an oil-in-water emulsion. The emulsion was cooled to ambient temperature and further processed by probe ultrasonication (5 min, 35% amplitude; Branson Sonifier 250 W/102C, Danbury, CT, USA) to reduce droplet size. The formulation parameters were systematically investigated to optimize nanoparticle characteristics, including Cutina HR: Sage oil mass ratios (80:20, 60:40, and 50:50%) and Cremophor RH 40 surfactant concentrations (2%, 3%, 4%).

Photon Correlation Spectroscopy (PCS) Investigation

Particle size analysis was conducted utilizing photon correlation spectroscopy (PCS) to evaluate the hydrodynamic diameter and size distribution of the nanoparticles. Measurements were performed using a Zetasizer Nano ZS90 (Malvern Instruments, UK), which provided quantitative metrics, including the Z-average (mean hydrodynamic diameter) and polydispersity index (PI), the latter reflecting the homogeneity of the particle population. Samples were diluted in double-distilled water at a concentration compliant with the manufacturer's specifications to ensure optimal

Table 1 DLX-SLCs and Their Size, PI, ζ Potential, and EE% Results

Formula	DLX (mg)	Cutina HR: Sage Oil Ratio	Cremophore RH 40	Tween 80 (mg)	Size (nm)	PI	ζP (mV)	EE %
F1	10	80:20	2%	100	215.5 ±3.7	0.461	−24.2±1.9	75.2±5.3
F2	10	80:20	3%	100	206.3 ±6.7	0.319	−23.8 ±2.4	76.6 ±2.9
F3	10	80:20	4%	100	178.1 ±4.6	0.342	−15.3 ±2.6	73.8 ±4.1
F4	10	60:40	2%	100	207.1 ±5.8	0.290	−24.9±1.7	75.8 ±4.8
F5	10	60:40	3%	100	120.6 ±3.9	0.212	−23.9±1.2	77.4±6.1
F6	10	60:40	4%	100	65.59 ±2.6	0.261	−18.2±1.4	75.1 ±5.3
F7	10	50:50	2%	100	143.2±3.1	0.192	−31.8±1.2	76.8 ±6.1
F8	10	50:50	3%	100	130.9±2.4	0.142	−28.4 ±2.3	79.9±3.8
F9	10	50:50	4%	100	56.8±2.9	0.331	−25.1 ±3.9	75.2±3.4

Abbreviations: DLX, Duloxetine; PI, poly dispersity index; ζ, zeta; EE, entrapment efficiency.

light scattering intensity. Surface charge characterization was concurrently performed via zeta potential analysis using the same instrument, offering insights into the colloidal stability of the formulations.

Encapsulation Efficiency (EE%) Estimation

The encapsulation efficiency (EE%), representing the proportion of DLX effectively retained within SLCs compared to the primary DLX input, was determined via a dialysis-based method. Briefly, 1 mL of the DLX-SLCs was enclosed in a cellulose dialysis tube (12–14 kDa molecular weight cutoff) and submerged in 100 mL of phosphate-buffered saline (PBS, pH 7.4, 37°C), ensuring sink conditions. The assembly was subjected to constant agitation (100 rpm, 4 h) to promote the passive diffusion of unencapsulated DLX into the surrounding medium. The unbound DLX concentration in the dialysate was measured using a UV-Vis spectrophotometer (UV-1601PC, Shimadzu, Japan) at a maximum absorbance wavelength (λmax) of 272 nm using the first derivative technique. Entrapment efficiency was derived using the following equation:

$$EE\,\% = \frac{Total\,DLX\,amount - free\,DLX\,amount}{Total\,DLX\,amount}\ \text{x}100$$

Optimization of Duloxetine Sage Lipid Carrier Nanoparticles

The formulation of DLX-SLCs was optimized through a comprehensive factorial experimental design (3^2) using Design-Expert® software (v.11, Stat-Ease Inc., USA). Two key independent variables, Cutina HR: Sage oil ratio (X_1: 80:20, 60:40, and 50:50%) and Cremophor RH 40 concentration (X_2: 2, 3, and 4%) were systematically evaluated for their impact on critical response variables: particle size (Y_1, nm), polydispersity index (Y_2), ζ potential (Y_3, mV), and EE (Y_4, %). A total of nine experimental runs, randomized and acted in triplicate, were conducted to mitigate batch-dependent variability. Response surface methodology (RSM) and analysis of variance (ANOVA) were applied to generate quadratic regression models, elucidate factor interactions, and identify optimal formulation parameters. The optimization criteria prioritized minimizing particle size and PI (<0.3) while maximizing EE, and ζ potential magnitude as modulus, ensuring colloidal stability. This data-driven approach facilitated the derivation of robust, statistically validated conditions for synthesizing DLX-SLCs with enhanced physicochemical performance.

In-vitro Release Study

The in vitro release of the optimized DLX-SLCs (F8) and pure DLX was assessed using a dialysis method. Samples containing (2 mg DLX) were sealed in a dialysis membrane (cutoff 12–14 KDa), submerged in vessels charged with 100 mL of phosphate buffer (pH 6.8) and maintained at 37 ± 0.5°C under continuous paddle rotation (50 rpm). Aliquots (1 mL) were periodically withdrawn through a 0.45 µm syringe filter (Merck Millipore, Germany), with immediate replenishment of fresh medium to preserve sink conditions. DLX concentration was quantified spectrophotometrically (UV-160A, Shimadzu, Japan) at λmax = 272 nm using the first derivative technique, with triplicate measurements ensuring methodological reproducibility. Release data were analyzed via DDSolver software, employing nonlinear regression to fit various kinetic models.[28]

Surface Morphology of Optimized Duloxetine Sage Lipid Carrier Nanoparticles

The morphological characteristics of the optimized DLX-SLCs (F8) were analyzed using transmission electron microscopy (TEM; JEM-2100, JEOL, Japan). Samples were prepared by depositing a diluted nanoparticle suspension onto a carbon-coated copper grid (300 mesh) via desiccation at ambient conditions. To enhance electron contrast, the grid was negatively stained with 2% (w/v) uranyl acetate solution for 60 seconds, followed by air-drying. TEM micrographs were acquired under high vacuum conditions at an accelerating voltage of 200 kV, enabling visualization of nanoparticle size, shape, and structural homogeneity.[29]

Synthesis of Chitosan Pimelate (CS-Pim) Polymer

Chitosan pimelate (CS-Pim) polymer was synthesized through a carbodiimide-mediated coupling reaction between chitosan (medium or low molecular weight, MMW or LMW) and pimelic acid at a 6:1 mass ratio (Table 2). Initially,

https://doi.org/10.2147/IJN.S569862

Table 2 Composition of Tested Buccal Films

Formula	CS M.W	CS: EDC Ratio	CS: Pimelic Acid Mass Ratio	Glycerin (%)	CS-Pim (%)
B1	L	1:0.1	6:1	3	3
B2	L	1:0.001	6:1	3	3
B3	M	1:0.1	6:1	3	3
B4	M	1:0.001	6:1	3	3

chitosan (CS) was dissolved in 1% (v/v) acetic acid, while pimelic acid was solubilized in ethanol. Ethyl-3-(3-dimethylaminopropyl) carbodiimide (EDC), acting as a crosslinker, was incorporated into the pimelic acid solution at chitosan-to-EDC mass ratios of 1:0.001 and 1:0.1. The mixture was stirred at ambient temperature for 25 min to activate the carboxylic acid moieties of pimelic acid. Subsequently, the activated solution was combined with the chitosan solution and agitated for 24 hours at room temperature to facilitate covalent conjugation. The chemical mechanism of the coupling reaction was illustrated in Supplementary 1. The resultant polymer was isolated by precipitation in 25% (v/v) ammonia solution, followed by centrifugation (5,000 rpm, 5 min) and repeated washing with purified water until a neutral pH (7.4) was attained. The purified CS-Pim was freeze-dried (Martin Christ GmbH, Germany) at −80°C for 84 hours to yield a dry, stable powder.[30]

Chitosan Pimelate Characterization via Fourier-Transform Infrared (FT-IR) Spectroscopy

Fourier-transform infrared (FT-IR) spectroscopy was employed to characterize structural distinctions among pimelic acid, CS and synthesized CS-Pim polymer variants. Spectral analyses were conducted using a Bruker ALPHA II spectrometer (Bruker AXS GmbH, Karlsruhe, Germany) with a spectral resolution of 4 cm^{-1} across the mid-infrared region (4000–400 cm^{-1}). Samples were prepared by homogenously dispersing the polymers in potassium bromide (KBr) pellets at a 1:200 (w/w) polymer-to-KBr ratio. This methodology enabled the identification of functional group alterations and molecular interactions, such as covalent bond formation between chitosan amino groups and pimelic acid carboxyl moieties, across the tested polymer derivatives.

Formulation of the Chitosan Pimelate Buccal Films

Buccal film preparations were developed using a solvent casting technique, employing different chitosan pimelate (CS-Pim) derivatives (Table 2) as bioadhesive matrices and glycerin as a plasticizing agent. For preliminary optimization, blank films (without DLX) were prepared by homogenously dispersing CS-Pim (3% w/w) in purified water under continuous stirring for 12 h at ambient temperature, followed by the incorporation of glycerin (3% w/w). The resultant polymeric dispersion was subjected to ultrasonication to eliminate entrapped air, cast into a 6 cm diameter plastic Petri dish, and thermally dried in an oven (40°C, 24 h), then at room temperature for 3 days. Post-drying, the patches were delicately peeled and encapsulated in a sealed jar to prevent moisture absorption.

Drug-loaded buccal films were fabricated by incorporating DLX-SLCs into chitosan pimelate (CS-Pim) matrices selected for their optimal buccal delivery performance, as determined by prior physicochemical characterization studies. The CS-Pim polymer, identified as the ideal formulation through rigorous evaluation parameters, was combined with DLX-SLCs at a targeted loading density of 6 mg per cm^2 of patch surface area. The mixture was homogenized under continuous magnetic stirring (12 h) to ensure uniform dispersion of DLX-SLCs within the polymeric matrix. Subsequent steps, including plasticizer addition, solvent casting, controlled drying, and precise sectioning into 1 cm^2 units, were executed per the standardized protocol established for blank film preparation.

Characterization of the Buccal Film Formulations

Physicochemical Properties Assessment of the Buccal Films

The physicochemical properties of buccal films (1 cm^2) were systematically evaluated. Film mass was determined using an analytical balance, with mean weight and standard deviation calculated from five replicates. Thickness uniformity was assessed via a digital micrometer (Guanglu, China) across five randomly selected films. For pH analysis, films were equilibrated in 5 mL PBS (pH 6.8) for 2 hours in sealed Petri dishes to prevent atmospheric interference, followed by pH measurement using a calibrated meter (Jenway 3510, Staffordshire, UK). Drug-containing films underwent identical pH testing to evaluate the influence of DLX on formulation acidity. Moisture loss was quantified by storing pre-weighed films (M_1) in desiccators containing anhydrous calcium chloride (3 days), with post-desiccation mass (M_2) used to calculate percentage moisture loss via the following Eq.:

$$\text{Moisture loss}(\%) = \frac{M1 - M2}{M1} X100$$

Mechanical properties were characterized using a Dynamic-Mechanical-Analysis (DMA) (DMA Q800 V21.1 Build 51, TA instruments, UK). Film strips were clamped and elongated at a constant rate of 0.1000 N/min to 18.0000 N until fracture. Tensile strength and elongation at break were derived from force-extension curves, with triplicate measurements ensuring statistical reliability.

The tensile strength (σ) and elongation at break (ε) % of the films were calculated using the following Eq:

$$\sigma = \frac{F}{A}$$

Where F is the force at failure (N), and A is the cross-sectional area of the film (cm^2).

$$\varepsilon\,(\%) = \frac{L_{break} - L_{initial}}{L_{initial}} X100$$

where L_{initial} is the initial length (mm), and L_{break} is the extended length at fracture (mm).

Drug Content Consistency Quantification

Drug-loaded films were fabricated by incorporating DLX at a standardized concentration of 6 mg/cm^2. For quantification, individual films (1 cm^2 surface area) were fully dissolved in 500 mL of phosphate-buffered saline (PBS, pH 6.8) under sonication (30 min). Post-dissolution, 1 mL aliquots were withdrawn, filtered through a 0.2 µm syringe filter (Nylon syringe filter, PRC) to remove particulate matter, and subjected to spectrophotometric analysis. DLX content was quantified using a UV-Vis spectrophotometer (UV-1601PC, Shimadzu, Japan) operating in first derivative mode, with absorbance measured at the λmax of 272 nm to enhance selectivity and minimize matrix interference.

Swelling Studies

This method provided insights into the fluid uptake and matrix expansion, critical for evaluating the film's ability to adhere to and hydrate the buccal mucosa. The swelling behavior of buccal films was quantified gravimetrically to assess their hydration capacity and mucoadhesive potential. Pre-weighed films (M_1) were immersed in 5 mL of PBS (pH 6.8) under controlled conditions (37 ± 1°C) for 2 h. At predetermined intervals, films were carefully removed, superficially blotted with filter paper to eliminate unabsorbed surface moisture, and reweighed (M_2). The experiment was conducted in triplicate to ensure reproducibility. The swelling index (%) was calculated using the following equation:

$$\text{Swelling index}(\%) = \frac{M2 - M1}{M1} X100$$

Ex-vivo Mucoadhesive Strength Evaluation

The ex vivo mucoadhesive strength of the buccal films was evaluated by a quantitative approach providing a direct measure of bioadhesion, reflecting the interfacial binding capacity between the film and mucosal membrane under simulated in vivo conditions, utilizing an adapted balance method. Freshly dissected rabbit buccal mucosal tissue was equilibrated with PBS (pH 6.8) to simulate physiological hydration. A film was affixed to the mucosal surface under constant pressure for 5 min to establish adhesive contact. Incremental weights of distilled water were then added until the patch detached from the mucosal substrate. The total mass of water (g) required to induce detachment was recorded.[29]

Surface Morphology of the Buccal Films

The surface morphology of buccal films was characterized using scanning electron microscopy (SEM). Beforehand imaging, samples were mounted on copper stubs and sputter-coated with a gold layer to enhance surface conductivity and mitigate electron charging artifacts. High-resolution micrographs were acquired using an SEM system (Oxford Instruments, UK) operated at an accelerating voltage of 20 kV in secondary electron detection mode.

Contact Angle Measurement of the Buccal Films

Contact angle measurements were conducted to evaluate the wettability of buccal films, utilizing Optical tensiometers (Theta flow, Biolin Scientific, UK). Films were securely affixed to a stage, and ultrapure water was vertically dispensed from a definite height onto the film surface at 25 ± 1°C. To account for surface heterogeneity, seven high-resolution images per droplet were captured 10 seconds post-dispensing under standard illumination, focal planes, and shading conditions. ImageJ software (v.1.53, NIH, USA) was employed to analyze droplet morphology, while contact angles were calculated via the sessile drop method. Triplicate measurements were performed across distinct film regions to ensure statistical robustness, and final values were derived from averaged data.[31]

Differential Scanning Calorimetry (DSC) Investigation

The thermal performance and stability of DLX, excipients (Cutina HR, sage oil, Cremophor RH 40, Tween 80), CS-Pim, and lipid-based formulations (plain SLCs, DLX-SLCs, and selected DLX-SLCs buccal film) were investigated via differential scanning calorimetry (DSC Q200, TA Instruments, USA). Before the assessment, the instrument was calibrated for temperature and enthalpy using high-purity indium (melting point: 156.6°C) and zinc (melting point: 419.5°C) standards. Samples (2–5 mg) were hermetically sealed in aluminum crucibles, with an empty crucible serving as a reference. Thermograms were recorded under a dynamic nitrogen atmosphere (50 mL/min) across a temperature range of 25–300°C, employing a heating rate of 10°C/min. This protocol enabled the identification of phase transitions, including melting, crystallization, and glass transitions, as well as incompatibilities between formulation components.[32]

Fourier-Transform Infrared (FTIR) Spectroscopy Inspection

FTIR spectroscopy was employed to investigate molecular interactions and compatibility among formulation components, including pure DLX, Cutina HR, sage oil, Cremophor RH 40, Tween 80, CS-Pim, plain SLCs, DLX-SLCs, and the selected DLX-SLCs buccal film. Spectra were acquired using a Bruker Alpha II FTIR spectrophotometer (Ettlingen, Germany) equipped with a diamond attenuated total reflectance (ATR) accessory. Before analysis, samples were uniformly compressed under hydraulic compression to ensure optimal contact with the ATR crystal. Scans were conducted across the mid-infrared region (4000–400 cm^{-1}) at a resolution of 4 cm^{-1}, with 32 co-added scans per sample to enhance signal-to-noise ratio.[33,34]

Ex-vivo Skin Permeation Studies of the Optimized Buccal Film

Ex vivo skin permeation studies were conducted using full-thickness abdominal skin harvested from male Wistar rats (200 ± 20 g) that were humanely euthanized using ketamine 80 mg/kg and xylazine 10 mg/kg intraperitoneally. The skin was surgically excised, treated with 0.3 N ammonium hydroxide solution to depilate hair and remove subcutaneous adipose tissue, and rinsed thoroughly with saline to eliminate residual alkali. Tissue integrity was verified visually, and samples with uniform thickness were selected. Afore experimentation, the skin was equilibrated in phosphate buffer (pH 7.4, 1 h) and air-dried. A 1 cm^2 section of the optimized DLX film was applied to the epidermal surface under gentle pressure and mounted in a Franz diffusion cell, with the stratum corneum facing the donor chamber and the dermal layer contacting the receptor compartment (300 mL PBS, pH 6.8, maintained at 37 ± 0.5°C under sink conditions). Aliquots (1 mL) were periodically withdrawn from the receptor medium, replaced with fresh PBS, and analyzed via UV spectrophotometry (λmax = 272 nm). Steady-state flux (J, $\mu g/cm^2/h$) was derived from the slope of the linear region of cumulative drug permeation (Q) versus time (t) profiles, providing quantitative insights into transdermal delivery kinetics.

Acute Toxicity Test

The OECD Guideline No. 423 was followed in toxicity studies.[35] Rats were given oral doses of 500, 1000, and 2000 mg/kg body weight of DLX-SLCs buccal film after being split into groups of three unisexual animals each. Following 48 hours of close monitoring, the animals were assessed for behavioural abnormalities such as paw licking, writhing, exhaustion, and decreased hunger, as well as any indications of fatality. Additionally, observations were made to verify regular activity and ensure there were no negative impacts on the animals' overall health.

In-vivo Studies Using Lipopolysaccharide (LPS)-Induced Depression Rat Model

Wistar rats (180–220 g) from the Sultan Qaboos University animal house were kept in stainless steel cages with a 12:12-hour light-dark cycle and controlled temperatures (22 ± 1°C). They were given unlimited access to water and food pellets. The recommendations of the National Institutes of Health Handbook for the Care and Use of Laboratory Animals were followed when conducting the research. The Sultan Qaboos University Standing Ethics Committee for Animal Use in Research gave the study ethical approval (Approval Code: SQU/EC-AUR/2024-2025/5).

The assessment of the enhanced antidepressant action of the drug and optimized formulation was achieved using a lipopolysaccharide (LPS)-induced rat model of depression-like behaviour. Five experimental groups, I, II, III, IV, and V ($n = 6$), were used in the study: negative control, positive control (LPS), Pure DLX, marketed DLX, and DLX-SLCs buccal film. The negative control was given saline orally and then IP saline after 30 min, while the positive control was given oral saline and then, after 30 min., administered with LPS intraperitoneally (LPS; Sigma-Aldrich, St. Louis, MO, USA) at a dose of 0.1 mg/kg once daily for 14 days.[36] Group III was given pure-DLX, 30mg/kg, after 30 min. of IP injection of LPS. Group IV was given Marketed-DLX, 30mg/kg, after 30 min. of IP injection of LPS. Then Group V was given DLX-SLCs Buccal Film 30 mg/kg after 30 min. of IP injection of LPS.

The tail suspension test (TST) and elevated plus maze (EPM) were used for behavioural evaluations. Ketamine 80 mg/kg and xylazine 10 mg/kg (given intraperitoneally) were used to establish profound anaesthesia in the rats before they were slaughtered. After being carefully removed, the brains were separated into two parts and cleaned with regular saline solution. While the first portion was maintained in 10% neutral buffered formalin for histopathological analysis, the second piece was snap-frozen in liquid nitrogen and kept at −80°C for a subsequent biochemical analysis.

Behavioural Analysis

To evaluate DLX-SLCs buccal film's antidepressant efficacy, behavioural despair models such as the Elevated Plus maze (EPM) and Tail suspension test (TST) were employed.

EPM consists of 4 arms in a cross shape with a central zone in the middle, placed approximately 45 cm above the ground. Two opposing standing arms have walls that are open at the top and do not interfere with the central zone. The test usually takes 10 min., enough to start the habituation process.[37] Rodents often evade open and brightly lit areas, although concurrently, they have a propensity to investigate novel environments. Consequently, the ratio of these conflicting stimuli was assessed.[38] The frequency of entrances into the open and closed arms and the central zone, and the total duration spent in these areas, were documented. Additional assessed indicators comprise raising, sniffing, grooming, and defecating. Prolonged duration in open arms signifies a diminished level of "anxiety" in the animal.[36]

The TST elicits behavior analogous to that observed in the Porsolt test. The advantage of this test against the Porsolt test was to eliminate the risk of hypothermia caused by water, as well as the possibility of assessing the strength and energy of the movement of the animal.[39] TST is primarily utilized in rodents, where the rat is suspended by its tail, with its body dangling in the air. The examination lasts around 6 min. and may be administered multiple times.[36] TST posits that the animal will attempt to evade stressful circumstances. After a while, the animal stops its struggle, resulting in immobility; prolonged stages of immobility indicate depressive behavior. The immobility phase is shortened following the introduction of antidepressants. Various strains of rats have distinct reactions to specific categories of antidepressants.

Sucrose Preference Test (SPT)

The SPT assessed hedonic response by providing animals with concurrent access to two bottles: one containing a 1% sucrose solution (1% w/v) and the other containing plain tap water. The percentage of sucrose preference, an indicator of anhedonia, was derived from sucrose solution intake and expressed as a proportion of total liquid consumption recorded over the last four days of the experimental period.

Measurement of ACTH, TNF-α, IL-1β, GABA, and Cortisol

Following careful collection into Vacutainer® Tubes containing EDTA, the blood extracted from the tail vein was centrifuged for 15 min at 4°C at 6000 rpm. Before analysis, the plasma was separated and kept at −80°C. Following the manufacturer's instructions, an ELISA test kit (Elabscience, Houston, TX, USA, Cat. No. E-EL-0160, E-EL-H0109, Cat. No. E-EL-H0149, and E-BC-K852-M, respectively) was used to measure the levels of ACTH, tumor necrosis factor-alpha (TNF-α), interleukin-1 beta (IL-1β), and Gamma-aminobutyric acid (GABA). Triplicate assays were made, results were represented as pg/mL, and the mean value for each sample was determined. Similarly, the cortisol ELISA kit (UNEB0007) was used to measure cortisol levels.

Measurement of Serotonin

Serum samples were obtained by centrifuging blood at 3000 × g for 10 min. and preserved at −20°C until analysis. Serotonin levels were quantified utilizing a competitive ELISA kit (Abcam, Cambridge, UK, Cat. No. ab133053) in accordance with the manufacturer's guidelines. Samples and standards were introduced in duplicate to antibody-coated microplate wells, treated with alkaline phosphatase-conjugated serotonin antigen and anti-serotonin antibody, and subsequently developed using p-nitrophenyl phosphate substrate. Absorbance was measured at 405 nm, and concentrations were ascertained using a standard curve.

Measurement of Antioxidant Enzymes

Superoxide dismutase (SOD) and malondialdehyde (MDA) kits from My BioSource, Inc. (San Diego, CA, USA) were measured by the colorimetric method, using the Bio Vision kit (Milpitas, CA, USA).

Histopathological Investigation

Following the rat's brain tissue samples' extraction, they were preserved in 10% neutral buffered formalin, gradually dried using a range of ethanol concentrations, cleaned in xylene, and then embedded in paraffin wax. After that, the tissue was divided into sections that were 5 µm thick and stained with hematoxylin and eosin. A light microscope was used to look for histopathological alterations in the stained sections.

Statistical Analysis

Minitab and Design-Expert tools were used for optimization analysis. Optimization analysis was conducted using one-way ANOVA at a significance threshold of $p < 0.05$. One-way ANOVA and Tukey's post hoc test were used for in vivo statistical analysis (GraphPad Software 8, Inc., San Diego, CA, USA). To quantify the precision of the findings, a 95% CI was employed. Using G-Power software version 3.1.9.4 (Fraz Faul, Germany), the sample size was computed to find the smallest number needed to test the study hypothesis.

Results and Discussion

Particle dimension is a vital quality parameter in nanopharmaceutical development, directly affecting formulation performance by altering pharmaceutical release, cellular uptake efficiency, dispersion stability, and medicinal bioactivity. Empirical evidence demonstrates that below 300 nm particle dimensions possess increased efficiency and greater cellular internalization due to improved mucosal penetration and decreased macrophage clearance, as supported by previous investigations.[40] The present study revealed that DLX-SLCs had a monomodal size distribution between 56.8 ± 2.9 nm and 207.1 ± 5.8 nm, as determined by DLS. A multivariate regression study revealed that the two independent variables (concentration of Cremophore RH 40 surfactant (X_1, % w/v) and Cutina HR: Sage oil ratio (X_2)) have significantly influenced ($p < 0.05$) particle diameter (Table 1). The interactive effects of these variables on particle size were further elucidated through three-dimensional response surface and contour plots (Figure 1A and B). Maximum particle diameters were observed at suboptimal surfactant concentrations (2% w/v) and a lipid phase ratio of 80:20 (Cutina HR: Sage oil), whereas incremental increases in Cremophore RH 40 to 4% w/v correlated with a pronounced reduction in hydrodynamic size. This inverse relationship aligns with the surfactant's role in lowering interfacial energy between the lipid and aqueous phases, enhancing emulsification efficiency during high-shear homogenization. At elevated concentrations, Cremophore RH 40 facilitates the formation of a stabilized monolayer at the lipid-water interface, promoting finer droplet subdivision and preventing coalescence.[41] Conversely, insufficient surfactant availability results in incomplete surface coverage, favoring particle aggregation and larger colloidal assemblies. Thus, optimum surfactant-to-lipid ratios can achieve nanoscale particle dimensions, a prerequisite for enhanced mucosal permeation and controlled drug release.

The ratio of solid lipid (Cutina HR) to liquid lipid (sage oil) exerted a statistically significant influence ($p < 0.05$) on the particle size of DLX-SLCs. Elevated proportions of Cutina HR correlated with increased particle diameters, attributed to the rigid crystalline structure of Cutina HR solid lipids, which promotes coalescence during the cooling and solidification stages of nanoparticle synthesis. Empirical evidence indicates that formulations with higher solid lipid content (eg, 80:20 solid-to-liquid lipid ratios) yield particles in the range of 150–281 nm, determined by the precise ratio employed.[42]

Conversely, incremental incorporation of sage oil (liquid lipid) induced a marked reduction in particle size, mediated by its capacity to modulate the lipid matrix's thermodynamic behavior. Liquid lipids lower the melting point and enhance the fluidity of the lipid phase, enabling finer droplet subdivision during high-energy homogenization. This improved emulsification facilitates the formation of smaller monodisperse colloidal structures, which are stabilized during solidification.[42]

PI is an important measure for evaluating the assembly and stability of NPs. It assesses the size diversity; a low PI shows a consistent size, whereas a high PI denotes size diversity. A PI value of below 0.3 is excellent because it implies homogenous particle sizes, which promote stability, eliminate aggregation, and assure reliable quality and efficacy of the NPs. The PI of the DLX-SLCs (Table 1) ranged between 0.142 and 0.461. PI exhibited no statistically significant correlation ($p > 0.05$) with the independent variables evaluated in the experimental design (Figure 1C and D). However, elevated liquid lipid (sage oil) content relative to the total lipid phase, combined with an optimized surfactant (Cremophore RH 40) concentration, significantly enhanced particle size uniformity, as evidenced by reduced PI values. This phenomenon is attributed to the liquid lipid's capacity to lower interfacial tension and improve emulsification efficiency, fostering monodisperse droplet formation during homogenization.[43] Concurrently, surfactant concentrations near CMC stabilized the lipid-aqueous interface, minimizing coalescence. These findings align with prior studies demonstrating that liquid lipid incorporation and surfactant optimization synergistically enhance colloidal homogeneity.[27]

The ζ potential of NPs is an additional significant measure of their stability, as it represents the possibility of clustering or distribution. It offers information about the surface potential and any changes performed to the NPs. Furthermore, it influences the intake of drugs by cells and plays an important role in drug delivery. The ζ potential of DLX-SLCs (Table 1) varied from −15.3 ±2.6 to −31.8 ±1.2 mV. The ζ potential of SLCs was significantly modulated by both independent variables, as depicted in the contour plots and response surface analysis (Figure 1E and F). Incremental increases in Cremophore RH 40 concentration (2% to 4% w/v) induced a marked reduction in zeta potential magnitude, attributable to the nonionic surfactant's capacity to neutralize surface charges via steric stabilization. Unlike ionic surfactants, Cremophore RH 40 lacks charged functional groups, instead forming a hydrated polymeric layer around particles that mitigates aggregation through spatial hindrance rather than electrostatic repulsion. At elevated concentrations, the dominance of steric stabilization over electrostatic interactions alters the colloidal equilibrium, potentially compromising long-term dispersion stability despite reduced surface charge.[44] The zeta potential of SLCs exhibited a direct relationship with the proportion of sage oil incorporated into the lipid matrix. This trend is likely mediated by ionizable acidic moieties within sage oil, which confer an enhanced negative surface charge to the nanoparticles. Comparative studies on lipid-based systems, including those utilizing black seed oil and linseed oil, confirm this phenomenon, demonstrating that liquid lipids with polar functional groups generate pronounced negative zeta potentials (typically ranging from −30 to −50 mV). Such elevated surface charges amplify electrostatic repulsion between particles, thereby enhancing colloidal stability by mitigating aggregation.[45,46] In contrast, formulations with higher solid lipid content displayed attenuated negative zeta potentials, indicative of reduced electrostatic stabilization. This decline arises from the nonpolar nature of solid lipids, which limits the availability of ionizable groups to contribute to surface charge. Consequently, SLCs dominated by solid lipids exhibit diminished stability compared to their liquid lipid-enriched

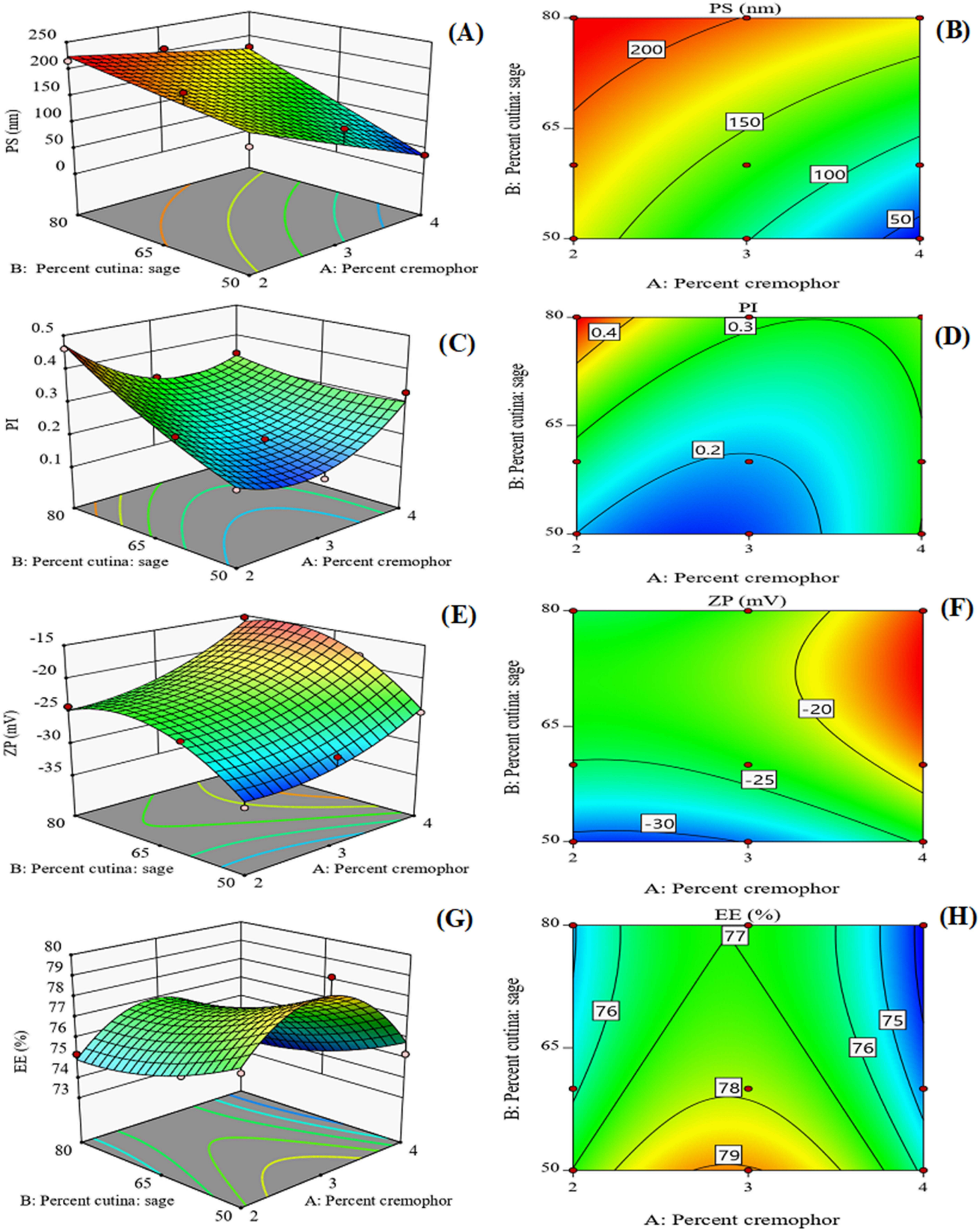

Figure 1 3D response surface analysis and Contour plots depicting the influence of Cutina HR: Sage oil ratio and surfactant (Cremophore RH 40) concentration on critical quality attributes of DLX-SLCs: (**A** and **B**) particle size (PS), (**C** and **D**) PI, (**E** and **F**) zeta potential (ZP), and (**G** and **H**) EE%.

counterparts, underscoring the critical role of lipid hydrophilicity in modulating interfacial charge dynamics and colloidal behavior.[47]

EE% serves as a critical determinant in the design of lipid-based nanocarriers, directly governing the therapeutic dose delivered by SLCs and ensuring clinical efficacy. The encapsulation efficiency of DLX within the SLCs is summarized in Table 1, demonstrating high values across all tested formulations (73.8% ±4.1 to 79.9% ±3.8). To optimize EE and mitigate premature release, the effects of two formulation variables, solid lipid-liquid lipid (Cutina HR: Sage oil) ratio and surfactant (Cremophore RH 40) concentration, on EE% were systematically investigated. The EE% of DLX was predominantly governed by both variables, with Cutina HR: Sage oil ratio exerting a more pronounced influence than Cremophore RH 40 concentration (Figure 1G and H). Elevated lipid content enhanced EE% due to DLX's higher partition coefficient in the lipid matrix, favoring thermodynamic affinity for the hydrophobic core over the aqueous phase. A significant dependence on the amount of sage oil was observed; formulations with reduced sage oil content exhibited significantly lower EE% than those enriched with liquid lipid. This trend underscores the pivotal role of sage oil in enhancing DLX entrapment, attributable to the drug's higher solubility in the liquid lipid phase relative to the solid matrix. Furthermore, formulations with elevated liquid lipid proportions yielded smaller nanoparticle diameters, as previously reported, which amplifies the interfacial surface area available for DLX partitioning during nanocarrier assembly. The synergistic interplay between lipid solubility and reduced particle size optimizes drug incorporation, aligning with established principles of lipid nanoparticle design where liquid lipids enhance drug loading and colloidal stability.[48] Conversely, a nonlinear relationship was observed between Cremophore RH 40 concentration and DLX encapsulation efficiency in the SLCs (Table 1). Incremental surfactant incorporation (from 2 to 3% w/v) enhanced EE%, likely due to improved interfacial stabilization and DLX partitioning into the lipid phase during nanoparticle assembly.[47] However, a paradoxical reduction in EE% occurred at the highest surfactant concentration (4% w/v), deviating from the anticipated trend. This attenuation may arise from micellar solubilization of liquid lipids by excess surfactant, which exceeds the critical micelle concentration (CMC). Such micellar entrapment reduces the available lipid phase for drug incorporation, diminishing overall EE%.[49] These findings revealed the surfactant's dual role as a stabilizer and a potential competitor in drug-loading dynamics, underscoring the necessity of optimizing surfactant-to-lipid ratios to balance emulsification efficacy and entrapment capacity.[41,50,51] It was proposed that 3% of Cremophore RH 40 is the optimal level of surfactant.

The desirability aspect is frequently employed in optimizing with multiple goals to determine the ideal formulation for various processes. The system consolidates several response factors into a singular combined desirability score, facilitating the simultaneous optimization of all aspects. It measures the appealing qualities of the preparations for every response factor. The adoption of the F8 formulation was determined by its optimal desirability factor of 0.821, warranting further assessment.

The in vitro release profiles of DLX from pure-DLX and optimized DLX-SLCs in phosphate-buffered saline (PBS, pH 6.8, 37°C) are presented in Figure 2A. Pure DLX exhibited rapid release, with 59.46% of the drug liberated within 1 h and near-complete release achieved by 24 h. This rapid dissolution of pure-DLX in PBS, pH 6.8, is attributable to its pH-dependent solubility profile. DLX, a weakly basic compound (pKa ≈ 9.7), undergoes amine protonation in neutral-to-acidic media, significantly enhancing its aqueous solubility at pH 6.8.[52] Empirical studies confirm near-complete solubility (>99%) in pH 6.8 PBS due to a favorable ionization equilibrium.[7] This high solubility accelerates drug dissolution and diffusion, explaining the observed burst release (59.46% within 1 h). In contrast, optimized DLX-SLCs demonstrated sustained release behavior with only 10.3% of DLX released within the initial hour, followed by prolonged, near-linear release reaching 61.8% at 24 h. The diminished burst release (≤15%) from SLCs confirms homogeneous dispersion of DLX within the lipid matrix, minimizing surface-associated drug fractions. This modulated release profile aligns with the lipid matrix-controlled liberation behavior, which is characteristic of lipid-based nanocarriers, where drug partitioning into the lipid core retards aqueous dissolution. A similar result was reported.[7]

The drug release mechanisms for pure-DLX and optimized DLX-SLCs were elucidated through kinetic modeling of dissolution data. Release profiles were fitted to established mathematical models, such as zero-order, first-order, Higuchi diffusion, and Korsmeyer-Peppas, using DDsolver software (Table 3). This quantitative approach identifies the governing release kinetics by determining the model that best describes the drug liberation process. Such mathematical

https://doi.org/10.2147/IJN.S569862

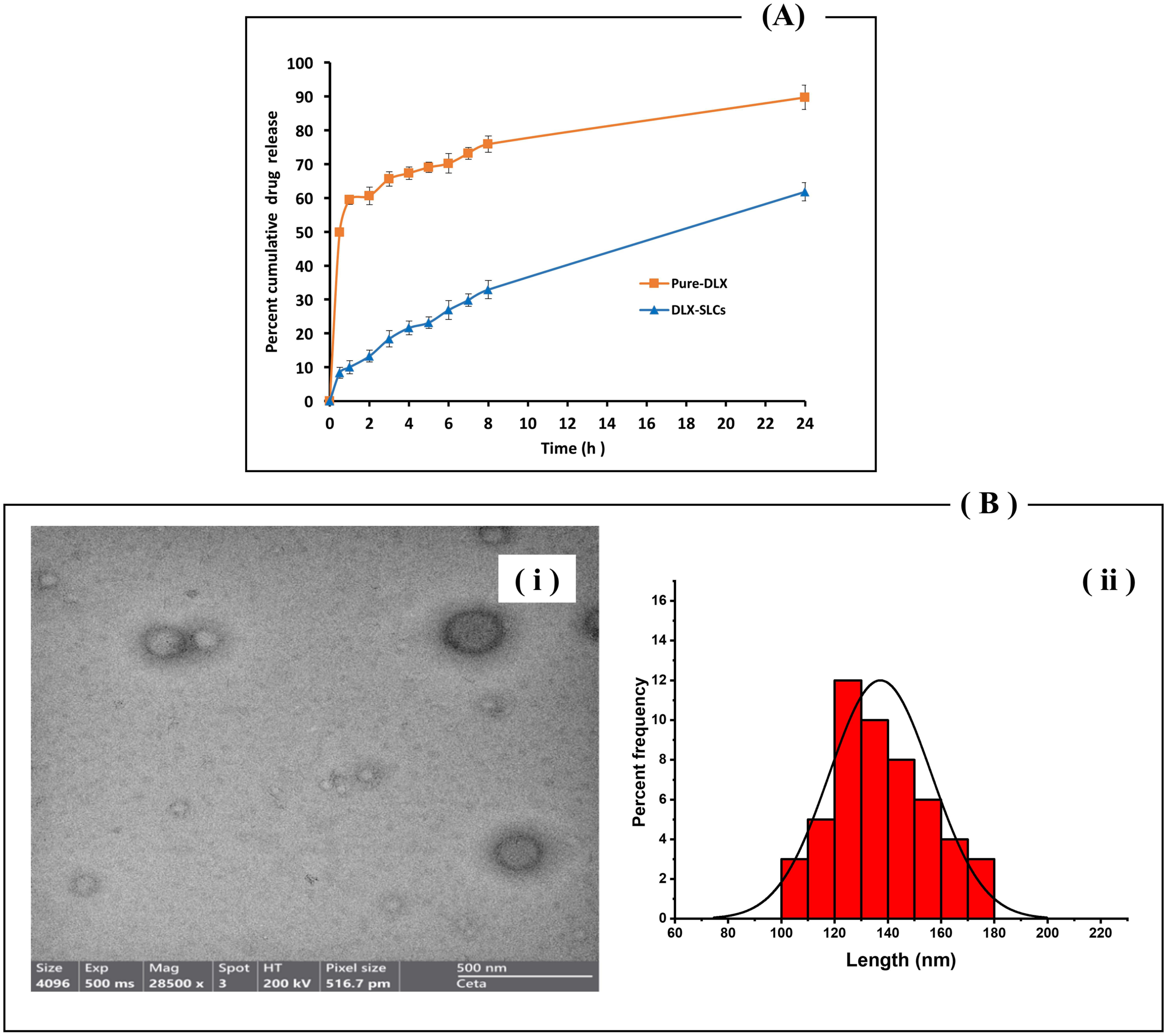

Figure 2 (**A**) In vitro DLX release profile from Pure-DLX and optimized DLX-SLCs and (**B**) TEM representations of optimized DLX-SLCs (scale bar = 500 nm) (i) and a histogram representing the presumed average hydrodynamic particle sizes derived from TEM (ii).

formalization provides critical insights into formulation performance while optimizing resource utilization: it discriminates between diffusion-controlled, erosion-mediated, and anomalous transport mechanisms.

The drug release mechanism from DLX-SLCs was diffusion-dominated, as evidenced by exceptional fit to the Korsmeyer-Peppas model (R^2 = 0.997), with a release exponent (n = 0.588) indicating anomalous (non-Fickian) transport, proposing an extended drug release mechanism that encompasses many mechanisms, including diffusion,

Table 3 Release Kinetics of DLX from Pure-DLX and Optimized DLX-SLCs

Formulation	Zero Order	First Order	Higuchi	Korsmeyer-Peppas		Hopfenberg	Baker-lonsdale
	R^2adj	R^2adj	R^2adj	R^2adj	N	R^2adj	R^2adj
Pure-DLX	0.630	0.347	0.058	0.995	0.144	0.267	0.612
DLX-SLCs	0.729	0.936	0.980	0.997	0.588	0.929	0.955

swelling, and erosion. The documented studies imply that $n < 0.43$ signifies diffusion-dependent liberation from nanosystems, but $n > 0.43$ suggests anomalous techniques with an escalating non-Fickian involvement as the n number rises. Our findings indicate that DLX-SLCs adhere to anomalous mechanisms characterized by a significant non-Fickian (case II transport) involvement. The observed behavior aligns with lipid-based carriers undergoing structural reorganization during dissolution, where interfacial hydration triggers progressive softening and erosion of the lipid matrix, thereby augmenting drug diffusion through aqueous pathways. Erosion kinetics modeling revealed that drug release from DLX-SLCs follows homogeneous, diffusion-controlled erosion mechanisms, as demonstrated by the superior fit to the Baker-Lonsdale model ($R^2 = 0.955$) compared to the Hopfenberg model.[17] This high correlation signifies uniform bulk erosion from spherical lipid matrices, consistent with the monodisperse morphology. The Baker-Lonsdale fit further confirms three governing mechanisms, constant diffusivity due to homogeneous drug distribution within the lipid core, stable spherical geometry during dissolution, and boundary layer-controlled aqueous penetration enabling gradual matrix erosion.[27,53]

Transmission electron microscopy (TEM) analysis of the optimized DLX-SLCs revealed the formation of monodisperse spherical nanoparticles (Figure 2Bi), as evidenced by the corresponding hydrodynamic size distribution histogram (Figure 2Bii). Particle dimensions obtained via TEM corroborated dynamic light scattering (DLS) measurements, confirming the precision of size characterization across orthogonal analytical techniques. Notably, the absence of particle aggregation or coalescence in TEM micrographs underscores the colloidal stability of the optimized DLX-SLCs, consistent with the low polydispersity index (PI < 0.3) derived from DLS analysis. The congruence between TEM and DLS data validates the robustness of the formulation process in achieving uniform nanoparticle morphology.[40]

Comparative FT-IR analysis of pure chitosan (CS), pure pimelic acid (Pim), and the CS-Pim conjugate polymer confirmed successful covalent modification through distinct spectral alterations (Figure 3A). Pure-Pim Figure 3Ai showed diagnostic peaks at 1681 cm^{-1} (carboxylic C=O stretch) and 1266 cm^{-1} (C-O stretch),[54,55] while pure-CS (LMW and MMW) (Figure 3Aii and iii, respectively) exhibited characteristic bands at 3332 cm^{-1} (O-H/N-H stretch), 1652 cm^{-1} (amide I), and 1587 cm^{-1} (amide II).[56] The different CS-Pim spectra (Figure 3Aiv, v, vi and vii) demonstrated critical changes including the disappearance of Pim's carboxylic C=O peak (1681 cm^{-1}), emergence of a new amide I band at 1644 cm^{-1}, shift in amide II to 1550 cm^{-1}, broadened N-H/O-H stretch (3309–3285 cm^{-1}), collectively evidencing amide bond formation between CS amine groups and Pim carboxyl moieties. Preservation of saccharide backbone vibrations (1024–1149 cm^{-1}) confirmed structural integrity post-modification. These spectral transitions, particularly the carbonyl frequency reduction, verify covalent conjugation while excluding physical mixture artifacts, establishing a robust foundation for functional polymer design. A similar result was reported for different CS derivatives using other dicarboxylic acids.[20]

The films were assessed for various parameters, including thickness, weight uniformity, pH, moisture loss, tensile strength, and elongation at break, to determine their appropriateness for buccal delivery. Buccal films must be sufficiently thin to avoid discomfort, as they will reside in the oral cavity for a designated duration. The film thicknesses were measured between 0.04 and 0.08 mm using an electronic micrometer. The weights of the films ranged from 11.1 to 28.7 mg. In accordance with reports, the augmented polymer molecular weight enabled the film to retain more water during the drying process.[57]

The weight and thickness of the films (Table 4) demonstrated concentration-dependent responses to EDC crosslinking, where higher EDC levels (0.1 M) typically increased both parameters due to enhanced polymer network density with more pimelic acid and restricted chain contraction during drying. Thus, formulations B2 and B4 (0.001 M EDC) exhibited reduced thickness (0.04 mm) compared to B1/B3 (0.1 M EDC) despite equivalent polymer concentration. This anomaly arises from EDC-mediated amide bond formation with the carboxylic group of pimelic acid, enabling denser polymer networks. Consequently, targeted low-level EDC crosslinking (0.001 M) achieves patient-preferred thinness (<0.05 mm) while preserving free amine groups for mucoadhesion.[23]

The surface pH of formulated buccal films was quantified to evaluate mucosal irritation potential, yielding values between 6.83 ± 0.04 and 7.08 ± 0.03 across all formulations (Table 4), with no statistically significant inter-group differences. This near-neutral range demonstrates physiological compatibility with the buccal mucosal environment (typical pH 6.3–7.4), thereby minimizing risks of epithelial irritation, salivary buffering disruption, or mucin denaturation.[58]

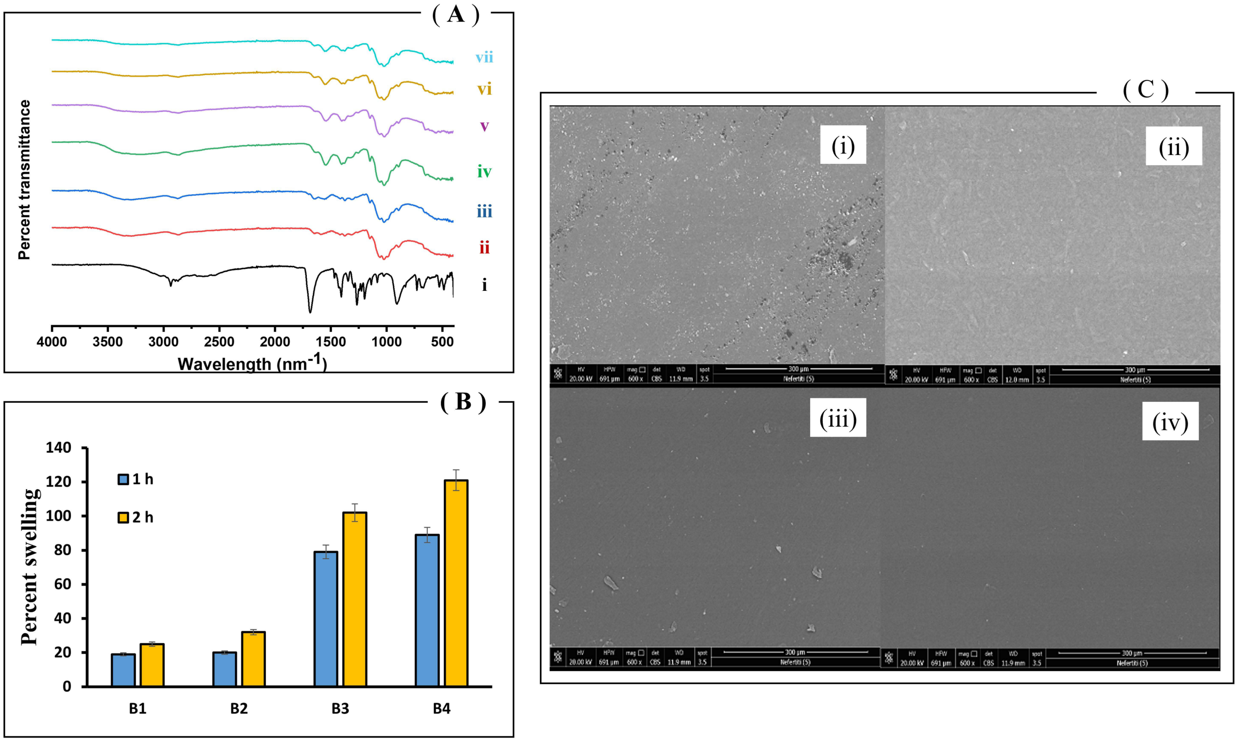

Figure 3 (**A**) FTIR spectra of (i) Pimelic acid, (ii) LMWT CS, (iii) MMWT CS, (iv) CS-Pim (B1), (v) CS-Pim (B2), (vi) CS-Pim (B3), and (vii) CS-Pim; (**B**) Swelling percent of buccal mucoadhesive film formulations and (**C**) Surface morphology of buccal mucoadhesive film formulations. (i) B1, (ii) B2, (iii) B3, (iv) B4.

The moisture loss of buccal films ranged from 13.19 ± 0.69% to 16.38 ± 0.59%, demonstrating a positive correlation with increasing polymer molecular weight (MW). MMW-CS exhibited greater moisture loss, attributed to greater free hydroxyl/amine groups per chain, increasing water capacity within the polymer, amplifying percentage loss due to higher initial hydration.[59]

Dynamic mechanical analysis (DMA) for tensile strength (Table 4) revealed that films incorporating MMW-CS exhibited significantly enhanced viscoelastic properties compared to LMW-CS at identical polymer concentrations (3% w/v). Specifically, MMW-CS film B4 demonstrated a higher tensile strength (10.07±0.34 N/cm^2 vs 3.08±0.24 N/cm^2 for LMW-CS (B2)) and greater elongation at break (109.9±7.3% vs 55.22±4.6%), attributable to the entanglement network density of MMW-CS chains forming more topological entanglements, increasing resistance to deformation.[60]

The DLX content consistency across buccal film formulations complied with pharmacopeial standards, as evidenced by analysis of 10 randomly selected films exhibiting DLX content within 85–115% of the labeled claim (mean: 98.19% ± 3.2% RSD). This narrow variability (≤6% RSD) satisfies regulatory requirements for dosage unit uniformity, ensuring consistent therapeutic dosing and batch-to-batch reproducibility. The observed homogeneity reflects optimized manufacturing parameters, guaranteeing that patients receive the intended DLX dose within ±5% accuracy.[29]

Optimal hydration capacity is critical for buccal films to ensure uniform drug release and mucosal absorption, as polymer swelling facilitates intimate mucoadhesive contact through transient polymer-mucin interactions. The swelling

Table 4 Physicochemical Properties, Drug Content, and Mucoadhesive Strength of Buccal Films

Formula	Weight Uniformity (mg)	Thickness Uniformity (mm)	pH	Moisture Loss (%)	Drug Content (%)	Tensile Strength (N/cm^2)	Elongation to Break (%)	Mucoadhesive Strength (g)
B1	18.3± 0.69	0.06±0.01	7.03±0.05	15.84±0.71	98.62±0.2	1.07±0.09	25.59±1.4	39.5 ± 1.32
B2	11.1± 0.73	0.04±0.03	6.83±0.04	13.19±0.69	96.32±0.6	3.08±0.24	55.22±4.6	42.9 ± 1.76
B3	28.7± 0.81	0.08±0.05	7.07±0.02	16.38±0.59	98.71±0.5	3.45±0.17	90.29±6.2	45.8± 1.61
B4	13.1±0.51	0.04±0.03	7.08±0.03	14.50±0.46	99.12±0.4	10.07±0.34	109.9±7.3	48.9± 2.38

index is directly influenced by polymer blend composition, triggering rapid matrix hydration upon mucosal contact, enabling weak bond formation and subsequent bioadhesion.[29] While controlled swelling is essential for buccal film mucoadhesion, excessive hydration compromises therapeutic efficacy by inducing patient discomfort and undermining structural integrity. Overswelling risks premature dissolution, disrupting cohesive matrix continuity, and weakening bioadhesive bonds; critical factors governing mucosal residence time and drug bioavailability. Optimal formulations must balance sufficient hydration for polymer-mucin interpenetration.[20] Formulation B4 exemplifies this equilibrium, achieving 124% swelling at 2 h while maintaining mechanical coherence through crosslinked polymer networks, thereby sustaining adhesion without compromising patient tolerance (Figure 3B). MMW-CS demonstrates significantly enhanced hydration capacity compared to LMW-CS, attributable to its optimal chain-length-dependent properties. MMW-CS chains possess sufficient length to deeply penetrate and form supramolecular entanglements within the mucin glycoprotein network, establishing robust interpenetrating polymer networks (IPNs) that enhance adhesion strength.[61] Concurrently, MMW-CS demonstrates greater cohesive strength within its polymeric matrix, resisting shear-induced disintegration at the mucosal interface; a critical attribute for maintaining structural integrity during physiological stress.[62] This is complemented by pronounced rheological synergy with mucin, where MMW-CS achieves maximal viscoelastic synergism through optimal charge density and chain entanglement, significantly increasing adhesive viscosity.[63] Crucially, MMW-CS balances solubility for interfacial interaction with cohesive viscosity for prolonged retention, avoiding the rapid dissolution seen in highly soluble LMW-CS. These properties collectively position MMW-CS as the preferred molecular weight range for sustained mucoadhesive efficacy, where balanced swelling sustains mucoadhesion without compromising structural integrity or patient comfort. Formulation B4 exhibited superior swelling (Figure 3B), attributable to synergistic hydrogen bonding through protonated amine groups ($-NH_3^+$) of chitosan in addition to the ionized carboxylic acid moieties ($-COO^-$) within its pimelate-conjugated polymer matrix. H-bonding forms reversible supramolecular crosslinks that stabilize the expanding network against dissolution. The resultant equilibrium between fluid absorption and mechanical integrity facilitates prolonged mucoadhesion essential for controlled buccal drug delivery, while avoiding overswelling-induced patient discomfort.[20]

Ex vivo mucoadhesive strength denotes the adhesion strength of a polymeric ingredient within the buccal film to the epithelial surface and mucus. Numerous factors influence mucoadhesive strength, including the degree of polymer swelling, variations in polymer molecular weight, contact duration, surface area, and the type of biological substrate employed. Mucoadhesion is a multi-faceted process encompassing moistening, penetration, adsorption, and establishing chemical bonds between the polymer and the buccal mucosal membrane. Increasing the polymer concentration or molecular weight enhances hydration levels and the quantity of linear chains, forming a robust network with mucin. This is due to hydrogen bonds, electrostatic attraction, or Van der Waals forces.[64,65]

In our investigation, the primary determinant of the mucoadhesive capability of positively charged chitosan is attributed to electrostatic interactions with oppositely charged mucin. An elevation in the content of polymers or molecular weight may also modify these interactions, accompanying mucoadhesion through enhanced physical entanglement. A researcher examined the bioadhesive characteristics of Amiloride buccal patches formulated with carbopol, chitosan, HPMC, and PVP polymers, discovering that chitosan demonstrated superior bioadhesive qualities compared to carbopol and HPMC, with bioadhesion enhancing as chitosan concentration rose.[66]

The mucoadhesive properties of CS derivatives are fundamentally governed by their chemical architecture, where swelling capacity serves as a critical determinant for mucosal adhesion efficacy. Enhanced hydration facilitates polymer chain expansion, enabling more profound interpenetration with mucin networks.[67] The mucoadhesive strength results for the buccal films varied from 39.5 ± 1.32 to 48.9± 2.38 g (Table 4). Formulation B4 (medium molecular weight chitosan crosslinked with 0.001 M EDC) demonstrated superior swelling capacity (124% in 2 h), correlating with its peak mucoadhesive strength (48.9 ± 2.38 g). This performance is attributable to optimal EDC crosslinking density preserved protonatable -NH_2 groups, enabling electrostatic binding to sialic acid residues in mucus; balanced crosslinking created expandable polymer matrices that increased contact area versus highly crosslinked analogues. In addition, MMW-CS polymer maximized chain entanglement efficiency while maintaining hydration equilibrium by allowing for more amine groups for electrostatic interaction.[60]

Scanning electron microscopy (SEM) analysis of DLX-SLCs-loaded buccal films revealed homogeneous, pore-free surfaces with compact microstructures (Figure 3C), indicating uniform distribution of formulation constituents and absence of phase separation. Formulation B4 (Figure 3Civ) exhibited superior surface integrity characterized by exceptional smoothness and structural continuity, attributable to synergistic hydrogen bonding between protonated amine groups ($-NH_3^+$) of MMW chitosan and ionized carboxylate moieties ($-COO^-$) of the pimelate conjugate. This interaction, enhanced by controlled solvent evaporation during casting and glycerol-mediated plasticization, promoted dense polymer chain reorganization while suppressing microcrack formation. The resultant morphological homogeneity maximizes interfacial contact area with the mucosal epithelium, enhancing mucoadhesive retention and drug delivery efficiency.[68]

Contact angle measurements (Figure 4A) quantitatively characterized the wettability characteristics of modified chitosan films, where lower angles ($\theta < 90°$) indicated enhanced hydrophilicity driven by protonated amine groups ($-NH_3^+$) and carboxylate moieties ($-COO^-$). Cross-linking of chitosan films significantly enhanced surface wettability, evidenced by contact angles ranging from 85.7° to 55.3°, confirming increased hydrophilicity. This may be due to cross-linking reorients polymer chains, exposing hydrophilic $-NH_2$/$-OH$ groups at the film-air interface, network formation disrupts crystalline domains, facilitating water interaction, in acidic media (eg, buccal pH 6.8), protonated amines ($-NH_3^+$) amplify surface hydration.[23] Formulation B4 (Figure 4Aiv) exhibited the lowest contact angle ($\theta = 55.3° \pm 2.3°$), confirming optimal surface energy for mucoadhesion.

The DSC thermal performance of pure DLX (Figure 4Bi) exhibited a singular endothermic event at 173.34°C ($\Delta H = 427.38$ J/g), corresponding to the melting transition of its crystalline lattice. This observation aligns with literature-reported values (170.5–172.2°C) for the thermodynamically stable anhydrous Form I polymorph of DLX.[7]

The DSC thermogram of Cutina HR (hydrogenated castor oil) (Figure 4Bii) exhibited a single sharp endothermic transition at 90.82°C ($\Delta H = 244.5$ J/g), corresponding to the melting of its crystalline triglyceride matrix in the thermodynamically stable β-polymorphic form. The high enthalpy value reflects >95% crystallinity, confirms homogeneous crystal structure, and lacks polymorphic impurities. This thermal behavior aligns with literature-reported properties for fully hydrogenated castor oil (85–90°C melting range).[69]

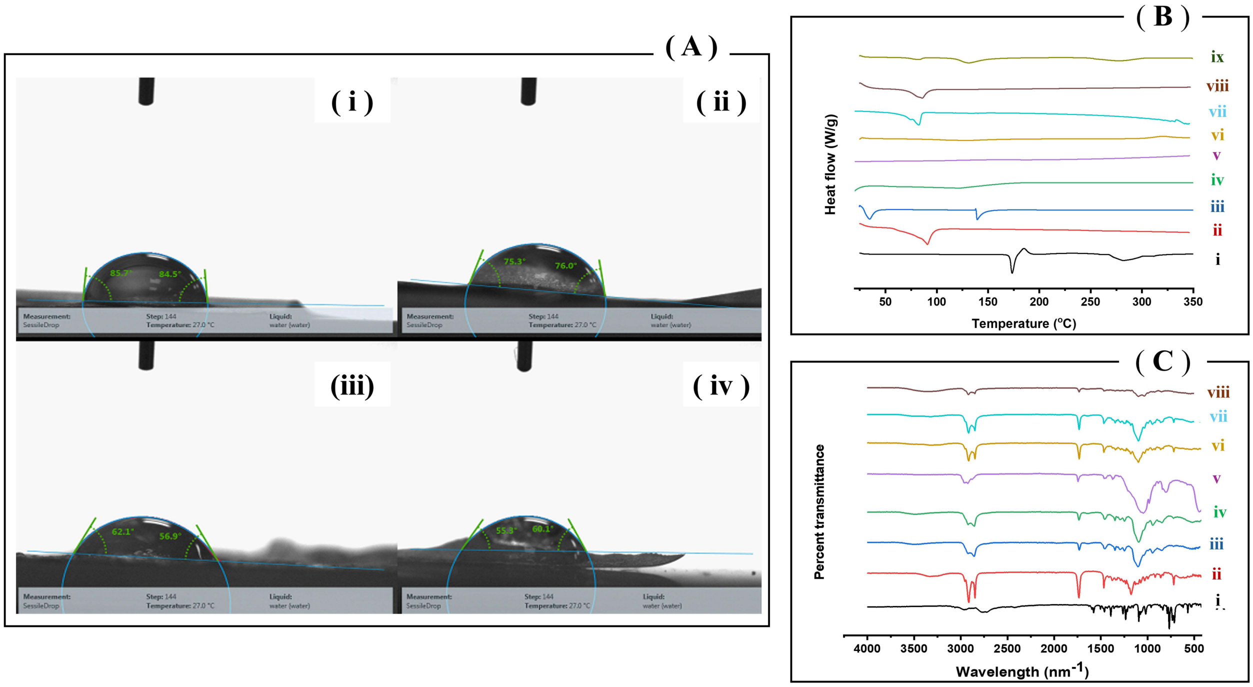

Figure 4 (**A**) The contact angle of buccal mucoadhesive film formulations. (i) B1, (ii) B2, (iii) B3, (iv) B4, (**B**) DSC of (i) DLX, (ii) Cutina HR, (iii) Cremophore RH 40, (iv) Tween 80, (v) sage oil, (vi) CS-Pim (B4), (vii) plain SLCs, (viii) DLX-SLCs and (ix) DLX-SLCs buccal film and (**C**) FTIR spectra of (i) DLX, (ii) Cutina HR, (iii) Cremophore RH 40, (iv) Tween 80, (v) sage oil, (vi) plain SLCs, (vii) DLX-SLCs, and (viii) DLX-SLCs buccal film.

DSC analysis of Cremophore RH 40 (Figure 4Biii) revealed two distinct endothermic transitions. A sharp melting peak at 34.54°C (ΔH = 105.95 J/g), corresponding to the melting of crystalline polyoxyethylene (PEG) domains in its hydrophilic moiety, followed by a decomposition event at 139.41°C (ΔH = 72.45 J/g), attributed to oxidative cleavage of ethoxylated fatty acid chains, causing its decomposition.[70,71]

The DSC analysis of Tween 80 (Figure 4Biv) lacks a distinct melting peak characteristic of a crystalline substance, comprising a mixture of esters and polyoxyethylene sorbitan derivatives, typically liquid or semi-solid at ambient temperature. The thermal phenomena detected in DSC pertain to softening and volatilization rather than discrete melting.[72,73]

The DSC examination of sage oil (Figure 4Bv) revealed a broad endothermic transition at 151.97°C (ΔH = 13.87 J/g), attributed to the evaporation of the investigated essential oils. Essential oils comprise numerous components, whose thermal effects during evaporation overlap, leading to a broad endothermic transition on the DSC curves.[74]

The DSC thermogram of the CS-Pim (Figure 4Bvi) exhibited two distinct endothermic peaks. The first peak at 127°C (ΔH = 68.73 J/g) attributed to the melting of crystalline domains formed by modified polymer chains. This peak suggests structural reorganization due to crosslinking, which enhances chain alignment and creates ordered regions. The second peak was detected at 320°C (ΔH = 31.31 J/g), corresponding to decomposition of the modified polysaccharide backbone. This elevated temperature (vs pure CS decomposition at 133.93 and pure pimelic acid at 269°C) confirms enhanced thermal stability from modifications.

The DSC examination of plain SLCs (Figure 4Bvii) exhibited a prominent endothermic transition at 82.44°C (ΔH = 94.5 J/g), representing an 8.4°C depression relative to bulk Cutina HR (90.82°C). This thermal shift arises from nanoconfinement effects reducing cooperative melting energy in lipid crystallites, coupled with structural reorganization induced by sage oil and surfactant-mediated disruption of hydrogen bonding networks.[27]

DSC thermogram of DLX-SLCs (Figure 4Bviii) revealed the complete absence of the characteristic crystalline melting endotherm of DLX (173.34°C, ΔH = 427.38 J/g), confirming molecular dispersion of DLX within the lipid matrix in a non-crystalline state. This loss of crystallinity indicates a transition to an amorphous phase stabilized by interactions with lipid matrix and surfactants. The amorphous solid dispersion state, thereby overcoming the limited bioavailability intrinsic to BCS Class II compounds like DLX.[33]

The DSC thermogram of DLX-SLCs buccal films (Figure 4Bix) exhibited two endothermic transitions. A primary peak at 131.26°C (ΔH = 194.56 J/g) and a secondary peak at 278°C (ΔH = 148.45 J/g), closely aligning with the CS-Pim polymer reference peaks (127°C and 320°C), yet with little shift. The displacement of the temperature transition arises from plasticizing the crystalline domains in CS-Pim, concurrently increasing transition enthalpy due to enhanced energy absorption during structural reorganization. The absence of DLX's crystalline melting endotherm (173.34°C) confirms complete amorphous drug dispersion within the lipid-polymer matrix.[27]

FTIR spectroscopy analysis of DLX (Figure 4Ci) reveals characteristic absorption peaks indicative of specific functional groups in its crystal. The N–H stretching vibration appears at 3096 cm^{-1}, confirming the presence of secondary amine functionalities. Aromatic C–H stretching vibrations are observed at 3061 cm^{-1}, while aliphatic C–H stretching absorptions occur at 2958 cm^{-1}. The carbonyl group from the sulfonamide moiety exhibits a strong absorption band in the region of 1599 cm^{-1}. Additionally, the C–N stretching vibration of the amine group is detected at 1264 cm^{-1}, and the C–O stretching from the ether linkage appears at 1234 cm^{-1}. Aromatic ring vibrations manifest as multiple bands at 1576 and 1463 cm^{-1}. These spectral features collectively aid in the structural identification and confirmation of DLX by highlighting key functional groups such as sulfonamides, aromatic rings, ethers, and nitrogen-containing moieties.[75]

The characteristic FTIR spectrum of Cutina HR (Figure 4Cii) exhibits distinct absorption bands that are indicative of its chemical composition. A prominent peak at approximately 1737 cm^{-1} corresponds to the strong ester carbonyl (C=O) stretching vibration, confirming the presence of ester linkages within the structure. A broad absorption band at 3328 cm^{-1} is attributed to O–H stretching vibrations, suggesting the presence of residual hydroxyl groups. Additionally, absorptions observed at 2915 cm^{-1} and 2847 cm^{-1} are assigned to C–H stretching vibrations from methylene groups in long aliphatic chains. The spectral features at 1176 cm^{-1} correspond to ester bonds' C–O stretching vibrations. Together, these IR signatures confirm the presence of aliphatic esters and glycerides, which are principal constituents of Cutina HR.[76]

The FTIR spectrum of Cremophor RH 40 (Figure 4Ciii) displays characteristic absorption bands that correlate with its molecular structure and functional groups. A broad and intense band at approximately 3496 cm^{-1} is attributed to O–H stretching vibrations, indicative of the presence of hydroxyl groups. Prominent absorption peaks at 2921 cm^{-1} and 2854 cm^{-1} correspond to C–H stretching vibrations arising from methylene and methyl groups in alkyl chains. A distinct peak around 1730 cm^{-1} confirms the presence of carbonyl (C=O) stretching from ester linkages within the molecule. Additionally, a band observed at 1110 cm^{-1} is assigned to C–O–C stretching vibrations, characteristic of ether bonds in polyethylene glycol (PEG) chains. These key spectral features collectively serve as diagnostic markers for confirming the chemical identity, structural integrity, and purity of Cremophor RH 40 in both analytical characterization and pharmaceutical formulation contexts.[44,77]

The FTIR spectrum of Tween 80 (Figure 4Civ) is representative of its molecular structure, which comprises a polyoxyethylene sorbitan backbone esterified with oleic acid. A prominent absorption band at approximately 1739 cm^{-1} corresponds to the C=O stretching vibration of the ester carbonyl group, serving as a key indicator of the ester functionality. The broad peak around 3492 cm^{-1} is attributed to O–H stretching vibrations arising from hydroxyl groups present in the polyoxyethylene chains. Characteristic aliphatic C–H stretching vibrations are observed at 2923 cm^{-1} and 2856 cm^{-1}, consistent with long-chain hydrocarbon moieties. Additionally, a distinct absorption at 1096 cm^{-1} corresponds to the C–O–C stretching vibration, confirming the presence of ether linkages within the polyoxyethylene segments. These diagnostic spectral features are crucial for the identification of Tween 80 in complex formulations and for verifying its incorporation into various drug delivery systems.[78,79] The FTIR spectrum of sage essential oil (Figure 4Cv) reflects its complex and diverse chemical composition, primarily of terpenoids and other volatile constituents. A prominent broad absorption band around 2989 cm^{-1} corresponds to O–H stretching vibrations, indicative of phenolic and alcoholic hydroxyl groups in compounds such as borneol and other oxygenated monoterpenes. Strong C–H stretching vibrations from aliphatic chains are observed at 2923 cm^{-1} and 2876 cm^{-1}, consistent with saturated hydrocarbon moieties. A distinct peak at 1745 cm^{-1} is attributed to C=O stretching vibrations arising from ester and ketone functionalities, characteristic of components like camphor and thujone derivatives. Additionally, aromatic C=C stretching vibrations manifest at 1463 cm^{-1}, while C–O stretching vibrations from ethers and alcohols appear at 1055 cm^{-1}. These spectral features correspond well with the major bioactive constituents of sage oil, including α-thujone, β-thujone, camphor, borneol, and 1,8-cineole, thereby confirming the presence of these key compounds through functional group-specific absorbance bands.[79,80]

The FTIR spectrum of a plain SLCs formulation (Figure 4Cvi) composed of Cremophor RH 40, Tween 80, and Cutina HR exhibits characteristic absorption bands that represent the combined contributions of these excipients. A broad O–H stretching vibration centered at 3363 cm^{-1} is attributed to hydroxyl groups present in the polyoxyethylene chains of both Cremophor RH 40 and Tween 80.[44] Prominent C–H stretching vibrations at approximately 2919 cm^{-1}and 2847 cm^{-1}are indicative of methylene and methyl groups from the long aliphatic chains found in all three components. A distinct carbonyl (C=O) stretching peak observed near 1732 cm^{-1} confirms the presence of ester linkages, predominantly originating from Cutina HR (a hydrogenated castor oil-derived glyceryl ester) and Tween 80. Additionally, a band at 1098 cm^{-1} corresponds to C–O–C stretching vibrations arising from the ethylene oxide units of the surfactants, further supporting the presence of polyether structures.[78] The FTIR spectrum also reveals characteristic peaks associated with sage essential oil, further supporting its incorporation into the SLC system. Notably, an absorption band near 1615 cm^{-1} corresponds to aromatic C=C stretching vibrations, while =C–H bending modes appear at 858 cm$^{-1.}$ These spectral features indicate the presence of terpenoid and phenolic constituents commonly found in sage essential oil.[80] When considered alongside the characteristic absorption bands of the lipid and surfactant components, these peaks collectively provide strong evidence for the successful formulation and compatibility of all constituents within the SLC matrix.[79]

The FTIR spectra obtained from DLX-SLCs, as presented in Figure 4Cvii, exhibited spectral patterns closely resembling those of the plain SLC formulations without duloxetine. This high degree of similarity suggests that the inclusion of DLX did not significantly alter the molecular arrangement or physicochemical integrity of the excipients comprising the SLC matrix. Furthermore, preserving characteristic absorption bands corresponding to the lipid and surfactant components indicates minimal interaction between DLX and the formulation constituents. These findings support the conclusion that DLX was successfully entrapped within the internal structure of the SLCs without compromising the structural stability of the delivery system.[27]

The FTIR spectra of the DLX-SLCs buccal film, as illustrated in Figure 4Cviii, revealed characteristic absorption bands similar to those observed in the optimized DLX-SLC formulation. However, a noticeable reduction in peak intensity was evident across the spectra. This attenuation in spectral intensity can be attributed to the dispersion and entrapment of the SLCs within the polymeric matrix of the buccal film. Incorporating SLCs into the film likely led to a dilution effect and restricted the vibrational freedom of functional groups, thereby reducing the overall absorbance signals. Moreover, the homogeneous distribution of lipid nanoparticles in the polymeric network may result in physical interactions, such as hydrogen bonding or van der Waals forces, between the lipid components and the polymer chains, which can further modulate the spectral response. These interactions and the encapsulation within a polymeric matrix are commonly associated with decreased FTIR peak intensity in composite drug delivery systems.

Regarding ex vivo skin permeation studies, the findings of the permeation study are presented in Table 5. The amount of DLX permeated through the mucosa was found to be 5242.5 ± 234.2 and 5626.8 ± 198.2 g cm^{-2} after 7 and 24 hours, respectively (Q_7 and Q_{24}). This indicates that the steady state was attained early. The rate of drug flux was calculated to determine the efficient enhancement of DLX permeation after DLX-SLCs CS-Pim film incorporation. The steady-state flux (J_{ss}) was found to be 31.849 ± 1.86 g cm^{-2} h^{-1}, which is a good improvement, indicating enhanced permeation of this drug. Previous study about permeation-enhanced duloxetine formulation reported similar trends of enhanced permeability, but to a lesser extent.[4,81] This enhancement was predicted and can be explained by the combined effect of sage nanoformulation (SLCs) and the mucoadhesive property of CS-Pim buccal film. The decreased particle size was reported to show a significant improvement in permeation-enhancing action, besides the presence of variable surfactants in SLC formulation, which act as permeation enhancers.[82,83] Also, chitosan and chitosan derivatives were reported to show enhanced permeability in buccal delivery systems owing to their mucoadhesive action that intimate the contact and increases the residence time.[20]

Acute toxicity intends to ascertain the lethal dose/concentration of a chemical that induces mortality in 50% of the examined subjects (LD/LC50) after short-term exposure.[84] Acute toxicity experiments were conducted. The results of the acute toxicity study in three groups of animals treated with up to 2000 mg/kg DLX-SLCs buccal film showed no signs of toxicity, behavioural changes, or mortality following treatment. The body weights of the animals remained relatively stable before and after treatment, with only minor variations: Group I (171±2 to 166±2 g), Group II (162±3 to 161±3 g), and Group III (170±2 to 172±3 g). The results suggest that the provided dosage of 30 mg/kg exhibits a favourable safety profile and poses no danger of acute toxicity.[85]

The EPM is a widely used behavioral assay for evaluating anxiety-related responses in rodents, based on their innate aversion to open and elevated spaces. Exposure to an unusual habitat in the EPM may cause modified behaviors in rodents, involving conflict, avoidance, social isolation, and terror.[86] The test records the time spent and the number of entries into the open (unwalled) and closed (walled) arms of the maze. Anxious rodents typically avoid the open arms and spend more time in the closed ones, whereas non-anxious rodents exhibit greater exploratory behavior by entering the open arms more frequently.[87,88]

All groups' animals underwent mild chronic stress, and their anxiolytic action was assessed. The stress-triggered rats (positive control) exhibited a substantial rise ($p < 0.001$) in the number of entrances in closed arms compared to open arms. The administration of DLX-SLCs buccal film reduced entrances in closed arms (Figure 5A) 1.62-fold, 1.32-fold, and 1.59-fold compared to the positive control, pure-DLX, and marketed-DLX, respectively. While entrances in open arms (Figure 5B) rose considerably ($p < 0.001$) 3.29-fold, 1.43-fold, and 1.59-fold compared to the positive control, pure-DLX, and marketed-DLX, respectively. Stress-triggered rats primarily allocated extra time to the closed arms (159.5 ± 3.6) sec. of the maze compared to the open arms (50 ± 4.8) sec. This conduct indicates their heightened uneasiness and anxiety in open environments. After treatment with DLX-SLCs buccal film, anxiety diminished, and the duration spent in closed arms (Figure 5C) diminished 1.6-fold, 1.26-fold, and 1.22-fold compared to the positive control, pure-DLX, and marketed-DLX, respectively. In contrast, the open arms (Figure 5D) expanded to 3.36-fold, 1.4-fold, and 1.29-fold compared to the positive control, pure-DLX, and marketed-DLX, respectively.

Table 5 Permeability Study Results (n = 3)

Formulation	J_{ss} (g cm^{-2} h^{-1})	Q_7 (g cm^{-2})	Q_{24} (g cm^{-2})	Permeability Coefficient (cm h^{-1})	Permeability ($t_{0\text{-}7}$) (%)	Permeability ($t_{0\text{-}24}$) (%)
DLX-SLCs buccal film	31.849 ± 1.86	5242.5 ± 234.2	5626.8 ± 198.2	3.54×10^{-3}	58.25	62.52

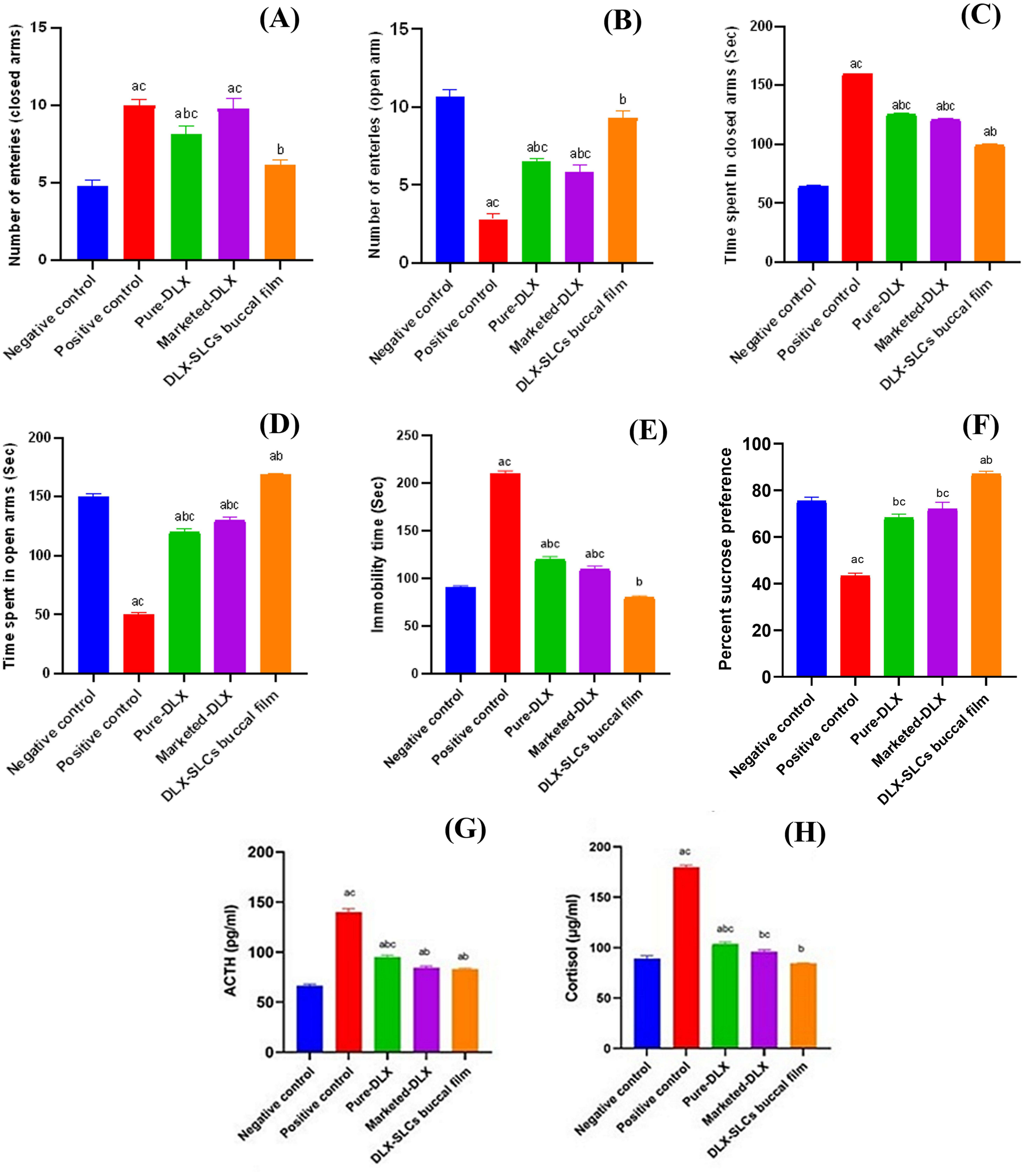

Figure 5 Effect of pure-DLX, marketed-DLX, and DLX-SLCs Buccal film on the number of entries in closed arms (**A**), open arms (**B**), and time spent on closed arms (**C**), and open arms (**D**), time of immobility (**E**), percent sucrose preference (**F**), ACTH (**G**) and cortisol (**H**) in depressed rats in depressed rats. Data were represented in mean ± SEM (n = 6). One-way ANOVA was used for statistical analysis, followed by Tukey's post hoc test.^{a}p<0.001 represents significance from the negative control group.^{b}p<0.001 represents significance from the positive control group.^{c}p<0.001 represents significance from the DLX-SLCs buccal film group.

The tail suspension test is one of the most used models for assessing antidepressant-like effects in rats.[89] The test is based on excessively hanging the tails, which results in a hemodynamically challenging stress situation. When depressed rodents are subjected to this inevitable stress of being hung by their tail, they will assume an immovable posture. The lack of escape-related behaviour is known as immobility.[90] Immobility behaviors provide a symptom of the psychological idea of "entrapment" associated with clinical depression. Consequently, the animal stops using proactive coping strategies for stressful situations.[91] The clinical studies show that sad persons often do not exert persistent effort, which is represented in a significant psychomotor deficiency, and may therefore be equivalent to this immobility.[92] Various antidepressants reverse immobility and promote the occurrence of escape-related behaviours.[93] The immobility test duration was documented during a six-minute assessment.

In the present investigation, in the TST test, the animals showed an immobility time of 210±10 sec in the stress-induced (positive control) group, which was considered significantly increased ($p < 0.001$) when compared to the negative control animals (90±8 sec). On treatment with DLX-SLCs buccal film, the immobility time dropped to 80±7 sec, which was considered significantly decreased ($p < 0.001$) as compared to stress-induced animals (Figure 5E).

Anhedonia, a primary symptom of depression, is evaluated using the sucrose preference test (SPT) behavioural test. It gauges how much rodents prefer a sweetened solution, typically sucrose, over unsweetened water; a lower preference denotes anhedonia. The idea behind this test is that animals that are depressed or acting anhedonistically will be less interested in foods and beverages that are typically appealing, such as sucrose.[94] The sucrose levels in pure-DLX, marketed-DLX, and DLX-SLCs buccal film-treated animals were raised significantly to 68.2 ±7.1, 72.04 ± 6.8, and 87 ± 5.2% compared to the positive animal groups (43.4 ±3.9%) (Figure 5F).

The results reported by the biochemical markers agreed with the preliminary behavioural tests. The hypothalamic-pituitary-adrenal (HPA) axis, which controls cortisol and ACTH, is frequently dysregulated in depression. This may contribute to the symptoms of depression by showing up as elevated cortisol levels and, in certain situations, elevated ACTH levels as well. Nevertheless, there is a complicated link between depression, cortisol, and ACTH.[94] The levels of ACTH and cortisol were recorded in all the animal groups. There was a significant reduction (70 ± 9 pg/mL and 80 ± 6 µg/mL; $p < 0.001$) in both the indices after the treatment with DLX-SLCs buccal film (Figure 5G and 5H).

Chronic physical or psychological stress can lead to oxidative/nitrative stress and inflammation, two important aspects of the pathophysiology of depression. In the hippocampus, these mechanisms also affect synaptic plasticity, neurotrophic support, and neurogenesis. Inhibiting the cascade of inflammation has been shown to offer new therapeutic alternatives for depression, especially for those suffering from treatment-resistant depression (TRD).[95] Structural imaging and brain neurochemistry studies show atrophic changes in the hippocampus, including low hippocampal cell number and volume loss, and impaired neurite development, when comparing individuals with multiple episodes of depression to healthy controls. These alterations could be brought on by anomalies in the HPA axis and a substantial rise in inflammatory markers such as IL-6, TNFα, and/or ROS. Inflammation and oxidative stress are reciprocally related to depression, according to several studies.[96]

The endotoxin lipopolysaccharide (LPS) acutely activates the peripheral innate immune system, leading to depressive-like behaviors in rat models. These effects include reduced saccharin consumption, increased immobility in the forced swim (FST) and TST tests, suppressed sexual behavior, diminished location preference, and elevated pro-inflammatory cytokine production. Long-term antidepressant treatment can reduce some of the symptoms of depression caused by LPS.[97]

The onset and severity of depression may be assessed by elevated levels of the inflammatory cytokines TNF-α and IL-1β. According to studies, people with depression frequently have higher blood levels of these cytokines than people in good health. These cytokines can impact mood regulation and brain function, which may exacerbate symptoms of depression.[94] Positive control showed an elevation ($p < 0.001$) in TNF-α levels (2.9-fold) and IL-1β (2.2-fold) compared to the negative control, confirming its expected inflammatory effect. These TNF-α levels displayed a 2.18-fold and 3.1-fold reduction ($p < 0.001$) in both the marketed-DLX and DLX-SLCs buccal film groups compared to the positive control, with a more pronounced effect compared to the group treated with pure-DLX (Figure 6A). Similarly, IL-1β displayed a 2.13-fold and 2.8-fold reduction ($p < 0.001$) in both the marketed-DLX and DLX-SLCs buccal film groups compared to the positive control, with a more noticeable effect compared to the group treated with pure-DLX 1.65-fold (Figure 6B).

GABA is a neurotransmitter that is essential for mood regulation and anxiety reduction. According to research, depression may be associated with abnormalities in GABA neurotransmission, specifically deficits in GABA levels. This implies that the brain's GABAergic pathways would make good targets for the creation of novel antidepressant medications.[94] By encouraging the activation of $GABA_A$ receptors, DLX-SLCs buccal film targets changes in neurotransmitter systems and GABA-induced inhibitory streams.[94] The levels of GABA were found to be increased ($^{c}p < 0.001$) 2.3-fold, 2.6-fold, and 3.5-fold in pure-DLX, marketed-DLX, and DLX-SLCs Buccal Film, respectively, as compared to the positive control group (Figure 6C).

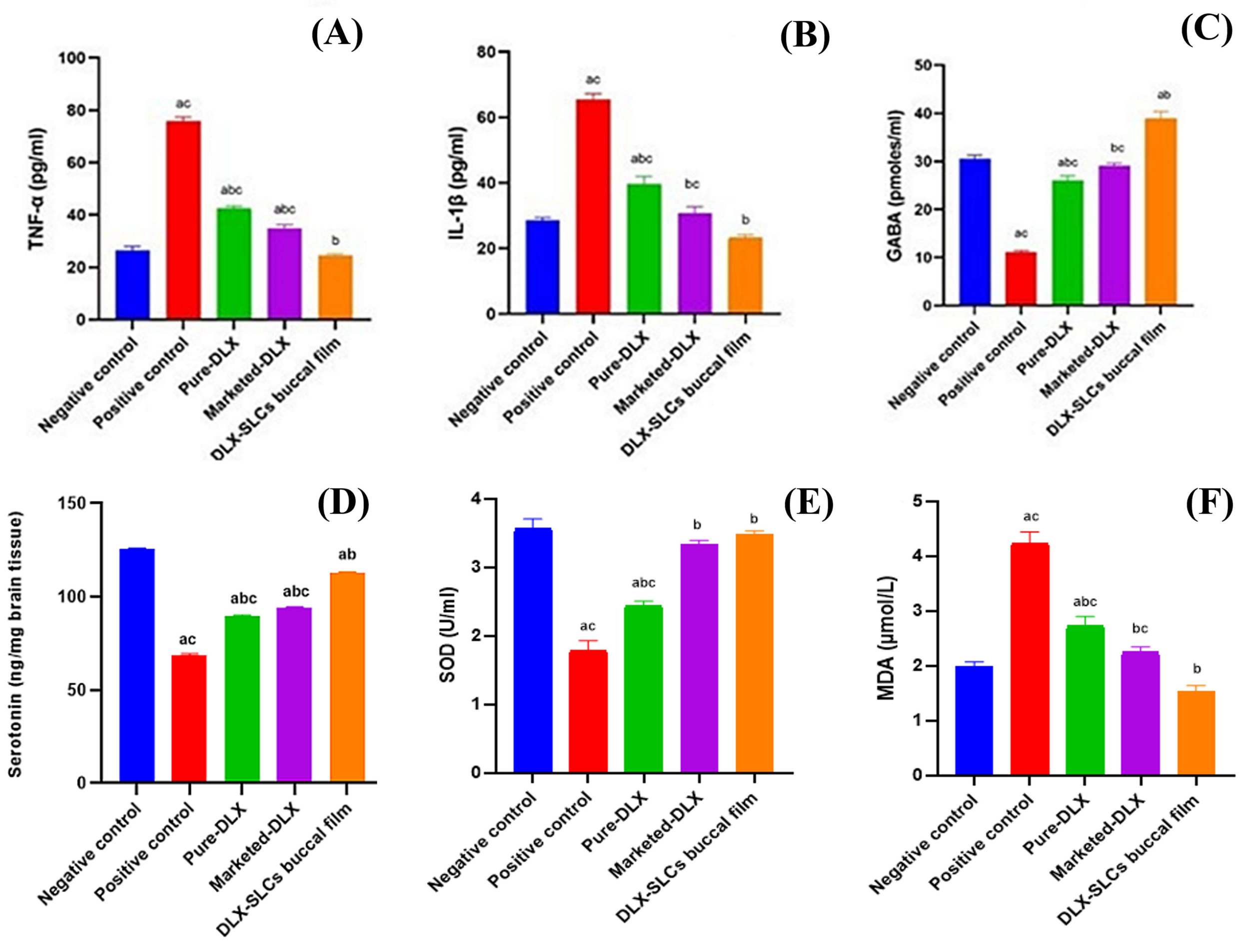

Figure 6 Effect of Pure-DLX, marketed-DLX, and DLX-SLCs Buccal film on TNF-α (**A**), IL-1β (**B**), GABA (**C**), serotonin (**D**), SOD (**E**), and MDA (**F**) in depressed rats. Data were represented in mean ± SEM (n = 6). One-way ANOVA was used for statistical analysis, followed by Tukey's post hoc test.^{a}p<0.001 represents significance from the negative control group.^{b}p<0.001 represents significance from the positive control group.^{c}p<0.001 represents significance from the DLX-SLCs buccal film group.

The findings of serotonin level revealed that the positive control showed a decrease in serotonin level (68.5 ng/mg) compared to the negative control (125.26 ng/mg). Pure-DLX and marketed-DLX significantly increased serotonin levels (89.9 ± 0.8 and 94.1 ± 1.0 ng/mg, respectively), confirming the serotonin–norepinephrine reuptake inhibition mechanism of action of DLX, which has been demonstrated to increase extracellular serotonin in rodent models of depression.[98] Nonetheless, these increases were significantly lower than those attained by the DLX-SLCs buccal film (112.7 ± 1.4 ng/mg), which basically raised serotonin levels to those of the normal group of controls (Figure 6D).

DLX-SLCs buccal film could increase brain bioavailability by mucoadhesive administration, circumventing hepatic metabolism and the blood-brain barrier with greater effectiveness than traditional oral preparations.[99] Nanoparticle-based delivery methods have been shown to defend the drug being delivered from enzymatic breakdown and enable tailored administration to the brain through the trigeminal or olfactory nerve pathways when supplied via the oral route.[100] These data clearly confirm the efficacy of DLX-SLCs Buccal Film as an innovative and superior approach for treating depression by more effectively increasing central serotonin levels compared to traditional formulations.

MDA and SOD are important components of the body's oxidative stress response and antioxidant defence mechanism, respectively. MDA is a sign of oxidative damage and lipid peroxidation, whereas SOD is an enzyme that counteracts superoxide radicals.[101] Elevated MDA levels indicate lipid peroxidation, a destructive mechanism whereby free radicals assault neuronal cellular membranes, leading to decreased functioning and mortality. The DLX-SLCs buccal film's ability to minimize MDA suggests strong anti-lipid peroxidative actions, protecting membrane integrity and reducing neuronal damage. This correlates with the observed neuroprotective and antidepressant-like effects, as oxidative stress is a known component of depression pathogenesis.[102]

SOD is a vital endogenous antioxidant enzyme that neutralizes superoxide radicals (O_2^{-}), preventing oxidative damage. The elevation of SOD activity shows enhanced endogenous antioxidant capability, counteracting the damaging effects of ROS in the brain.[103] Since depression and anxiety disorders are associated with lower SOD activity, the DLX-SLCs buccal film's ability to restore SOD levels supports its antidepressant and anxiolytic efficacy.

In the current study, DLX-SLCs buccal film has antioxidant qualities that include raising SOD while decreasing lipid peroxidation (malondialdehyde, MDA, content). With the treatment of DLX-SLCs buccal film, the SOD values increased by 90.05 ± 7.3 and 57.23 ± 3.5% compared with the positive control, pure-DLX, respectively (Figure 6E). While the MDA decreased by 61.14 ± 4.8, 38.02 ± 3.5, and 24.72 ±1.8% compared with the positive control, pure-DLX, and marketed-DLX, respectively (Figure 6F).

A histological analysis of brain tissue segments from several groups was performed to evaluate alterations in morphology or structural modifications. Hippocampus sections within the negative control had normal neurons with vesicular pale nuclei (black arrow) (Figure 7A), while the positive control (Figure 7B) shows degenerated neurons (green arrow) and atrophy of the tissue around the degraded neurons (black arrow). There are some regenerative changes in pure-DLX (Figure 7C), and these regenerative changes become obvious with marketed-DLX (Figure 7D). In DLX-SLCs buccal film (Figure 7E), the regenerative changes become very clear in the neurons (black arrow).

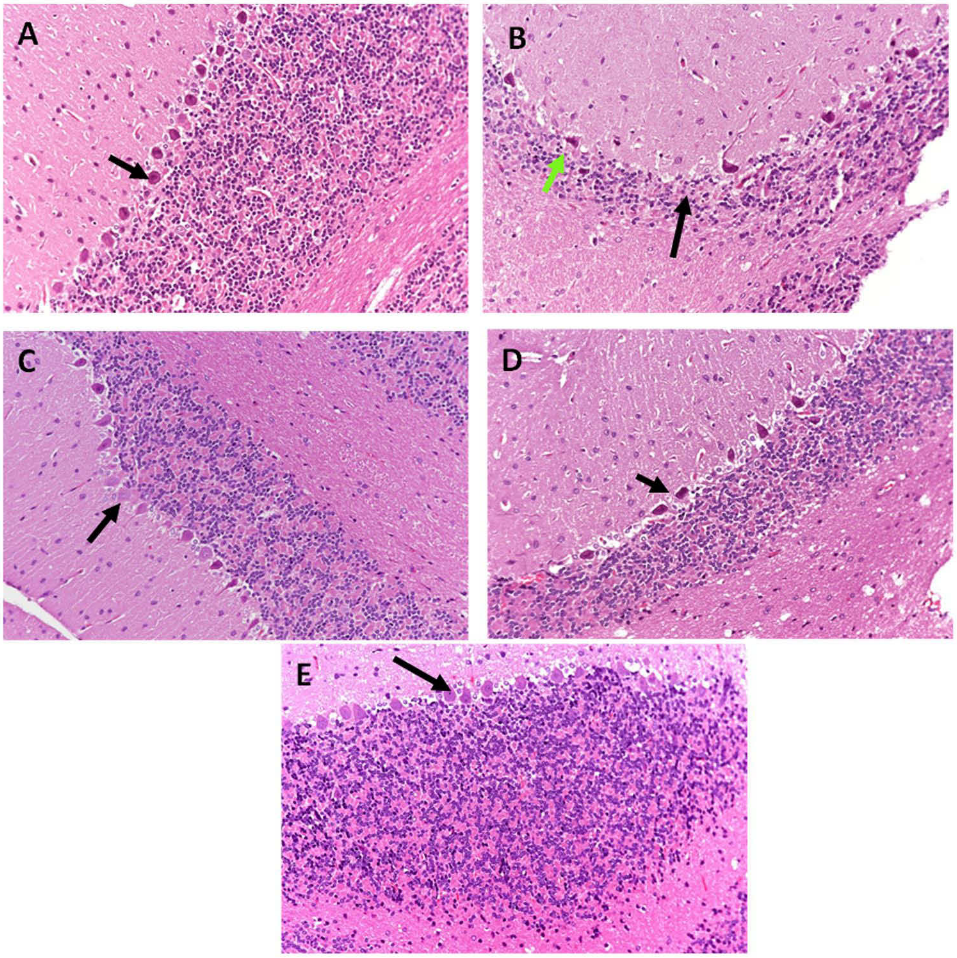

Figure 7 The effect of Pure-DLX, marketed-DLX, and DLX-SLCs Buccal Film on the hippocampal regions. Representative pictures of hippocampal regions from the negative control (**A**) with vesicular pale nuclei (black arrow), positive control LPS (**B**) shows degenerated neurons (green arrow) and atrophy of the tissue around the degraded neurons (black arrow), Pure-DLX (**C**), Marketed-DLX (**D**), and DLX-SLCs buccal film (**E**) shows regenerative changes very clear in the neurons (black arrow).

Conclusion

This study introduces DLX–SLCs–loaded chitosan–pimelate (CS–Pim) buccal films as a novel mucoadhesive nanoplatform for effective depression management. The formulation strategically combines the brain-targeting potential of sage lipid carriers with the mucoadhesive and sustained-release properties of the newly synthesized CS–Pim polymer, offering a unique dual-delivery approach.

The developed system demonstrates clear advantages over conventional oral DLX therapy, including improved effectiveness, avoiding first pass metabolism, prolonged retention, and potential neuroprotective action, while reducing systemic side effects. Beyond its therapeutic promise, this work highlights the innovative use of CS–Pim as a versatile mucoadhesive polymer that may be extended to other neuropsychiatric or transmucosal drug delivery systems.

Future studies will focus on long-term safety evaluation and clinical translation to further validate the potential of this buccal nanoplatform as an advanced, patient-friendly alternative for central nervous system drug delivery.

Data Sharing Statement

The data supporting the results of this research can be retrieved from the corresponding author on reasonable demand.

Ethical Approval

The recommendations of the National Institutes of Health Handbook for the Care and Use of Laboratory Animals were followed when conducting the research. The Sultan Qaboos University Standing Ethics Committee for Animal Use in Research gave the study ethical approval (Approval Code: SQU/EC-AUR/2024-2025/5).

Acknowledgments

The authors thank the Deanship of Graduate Studies and Scientific Research at University of Bisha for supporting this work through the Fast-Track Research Support Program.

Author Contributions

All authors made a significant contribution to the work reported, whether that is in the conception, study design, execution, acquisition of data, analysis and interpretation, or in all these areas; took part in drafting, revising or critically reviewing the article; gave final approval of the version to be published; have agreed on the journal to which the article has been submitted; and agree to be accountable for all aspects of the work.

Funding

The authors assert no external financial sources.

Disclosure

The authors disclose no financial interests or personal connections that could be perceived as competing interests.

References

1. Abd-Elal RMA, Essawy AM, Salem MA, et al. Formulation, optimization, in-vivo biodistribution studies and histopathological safety assessment of duloxetine HCl-loaded ultra-elastic nanovesicles for antidepressant effect after intranasal and transdermal delivery. *Int J Pharm X*. 2023;6:100194. doi:10.1016/j.ijpx.2023.100194
2. Tawfik MA, Mohamed MI, Tadros MI, El-Helaly SN. Low-frequency sonophoresis as an active approach to potentiate the transdermal delivery of agomelatine-loaded novasomes: design, optimization, and pharmacokinetic profiling in rabbits. *AAPS Pharm Sci Tech*. 2021;22:1–15. doi:10.1208/s12249-021-02147-y
3. Rodrigues-Amorim D, Olivares JM, Spuch C, Rivera-Baltanás T. A systematic review of efficacy, safety, and tolerability of duloxetine. *Front Psychiatry*. 2020;11:554899. doi:10.3389/fpsyt.2020.554899
4. Salem HF, Ali AA, Rabea YK, El-Ela FIA, Khallaf RA. Glycerosomal thermosensitive in situ gel of duloxetine HCl as a novel nanoplatform for rectal delivery: in vitro optimization and in vivo appraisal. *Drug Deliv Transl Res*. 2022;12(12):3083–3103. doi:10.1007/s13346-022-01172-z
5. Kondiah PPD, Mdanda S, Makhathini SS, Rants'o TA, Choonara YE. Development of a eudragit-chitosan nanosystem for the ph-dependent transport of duloxetine to the brain: synthesis, characterization and in silico modeling analysis. *Nanofabrication*. 2022;7.
6. Zewail MB, El-Gizawy SA, Asaad GF, Shabana ME, El-Dakroury WA. Chitosan coated clove oil-based nanoemulsion: an attractive option for oral delivery of leflunomide in rheumatoid arthritis. *Int J Pharm*.

7. Patel K, Padhye S, Nagarsenker M. Duloxetine HCl lipid nanoparticles: preparation, characterization, and dosage form design. *AAPS Pharm Sci Tech*. 2012;13:125–133. doi:10.1208/s12249-011-9727-6
8. Maliki I, Es-Safi I, El Moussaoui A, et al. Salvia officinalis and Lippia triphylla: chemical characterization and evaluation of antidepressant-like activity. *J Pharm Biomed Anal*. 2021;203:114207. doi:10.1016/j.jpba.2021.114207
9. Dos Santos ÉRQ, Maia JGS, Fontes-Júnior JGS, Do Socorro Ferraz Maia C, Dos Santos ÉRQ, Do Socorro Ferraz Maia C. Linalool as a therapeutic and medicinal tool in depression treatment: a review. *Curr Neuropharmacol*. 2022;20(6):1073–1092. doi:10.2174/1570159X19666210920094504
10. Mixcoatl-Zecuatl T, Jolivalt CG. A spinal mechanism of action for duloxetine in a rat model of painful diabetic neuropathy. *Br J Pharmacol*. 2011;164(1):159–169. doi:10.1111/j.1476-5381.2011.01334.x
11. De Sousa DP, Silva RHN, Silva EF, Gavioli EC. Essential oils and their constituents: an alternative source for novel antidepressants. *Molecules*. 2017;22(8):1290. doi:10.3390/molecules22081290
12. Du W, Chen H, Gróf I, et al. Antidepressant-induced membrane trafficking regulates blood-brain barrier permeability. *Mol Psychiatry*. 2024;29(11):3590–3598. doi:10.1038/s41380-024-02626-1
13. Singh G, Sarwal A, Sharma S, Prasad P, Kuhad A, Ali W. Polymer-based prolonged-release nanoformulation of duloxetine: fabrication, characterization and neuropharmacological assessments. *Drug Dev Ind Pharm*. 2021;47(1):12–21. doi:10.1080/03639045.2020.1851240
14. Peddapalli H, Dudhipala N, Chinnala KM, Banala N. Transmucosal delivery of duloxetine hydrochloride for prolonged release: preparation, in vitro, ex vivo characteri-zation and in vitro-ex vivo correlation. *Int J Pharm Sci Nanotech*. 2018;11(5):29–4258.
15. Macedo AS, Castro PM, Roque L, et al. Novel and revisited approaches in nanoparticle systems for buccal drug delivery. *J Control Release*. 2020;320:125–141. doi:10.1016/j.jconrel.2020.01.006
16. Jacob S, Nair AB, Boddu SHS, Gorain B, Sreeharsha N, Shah J. An updated overview of the emerging role of patch and film-based buccal delivery systems. *Pharmaceutics*. 2021;13(8):1206. doi:10.3390/pharmaceutics13081206
17. El-Dakroury WA, Zewail MB, Mansour MA, et al. A novel furo [2, 3-d] pyrimidine-based chalcone derivative (MMK-1931) loaded chitosomes as a potential cancer therapy in an Ehrlich ascites tumour model. *J Drug Target*. 2025;33:1914–1931. doi:10.1080/1061186X.2025.2530651
18. El-Dakroury WA, Asaad GF, Shabana ME, et al. Famotidine-loaded chitosan hybridized fibroin nanoparticles exhibit outstanding efficacy in ameliorating peptic ulcer. *Int J Biol Macromol*. 2025;327:147321. doi:10.1016/J.IJBIOMAC.2025.147321
19. Zewail MB, El-Gizawy SA, Asaad GF, El-Dakroury WA. Development of famotidine-loaded lecithin-chitosan nanoparticles for prolonged and efficient anti-gastric ulcer activity. *J Drug Deliv Sci Technol*. 2024;91:105196. doi:10.1016/j.jddst.2023.105196
20. Arpa MD, Okur NÜ, Gök MK, Özgümüş S, Cevher E. Chitosan-based buccal mucoadhesive patches to enhance the systemic bioavailability of tizanidine. *Int J Pharm*. 2023;642:123168. doi:10.1016/j.ijpharm.2023.123168
21. Mura P, Maestrelli F, Cirri M, Mennini N. Multiple roles of chitosan in mucosal drug delivery: an updated review. *Mar Drugs*. 2022;20(5):335. doi:10.3390/md20050335
22. Kuroiwa T, Okuyama Y, Kanazawa A. Improved stability of the palm oil-in-water emulsion via the surface modification of droplets with a chitosan-casein complex layer. *Jpn J Food Eng*. 2021;22(4):105–115. doi:10.11301/jsfe.21598
23. Sharma D, Singh J. Synthesis and characterization of fatty acid grafted chitosan polymer and their nanomicelles for nonviral gene delivery applications. *Bioconjug Chem*. 2017;28(11):2772–2783. doi:10.1021/acs.bioconjchem.7b00505
24. Tabatabaei M, Rajaei A, Hosseini E, Aghbashlo M, Gupta VK, Lam SS. Effect of type of fatty acid attached to chitosan on walnut oil-in-water Pickering emulsion properties. *Carbohydr Polym*. 2022;291:119566. doi:10.1016/j.carbpol.2022.119566
25. Burchacka E, Potaczek P, Paduszyński P, Karłowicz-Bodalska K, Han T, Han S. New effective azelaic acid liposomal gel formulation of enhanced pharmaceutical bioavailability. *Biomed Pharmacother*. 2016;83:771–775. doi:10.1016/j.biopha.2016.07.014
26. Sedyakina NE, Zakharov AN, Krivoshchepov AF, et al. Effect of carbon chain length of dicarboxylic acids as cross-linking agents on morphology, encapsulation, and release features of protein-loaded chitosan microparticles. *Colloid Polym Sci*. 2017;295:1915–1924. doi:10.1007/s00396-017-4171-0
27. El-Dakroury WA, Said AR, Abdel Mageed SS, et al. Rivaroxaban loaded lipid carriers integrating EPA oil: a novel paradigm in drug repurposing for navigating colon targeted oral treatment for ulcerative colitis. *J Drug Deliv Sci Technol*. 106985; doi:10.1016/j.jddst.2025.106985
28. El-Dakrouri WA, Ibrahim HK, Ghorab MK, Ghorab MM. Enhancement of the intranasal delivery of insulin via a novel mucoadhesive Carbopol gel. *J Pharm Pharmacol*. 2010;62(7):866–872. doi:10.1211/jpp.62.07.0007
29. Zewail MB, F.Asaad G, Swellam SM, et al. Design, characterization and in vivo performance of solid lipid nanoparticles (SLNs)-loaded mucoadhesive buccal tablets for efficient delivery of Lornoxicam in experimental inflammation. *Int J Pharm*. 2022;624:122006. doi:10.1016/j.ijpharm.2022.122006
30. Arpa MD, Okur NÜ, Gök MK, Cevher E. Chitosan-based buccal mucoadhesive bilayer tablets enhance the bioavailability of tizanidine hydrochloride by bypassing the first-pass metabolism. *J Drug Deliv Sci Technol*. 2024;97:105739. doi:10.1016/j.jddst.2024.105739
31. Kulkarni PS, Deshmukh PG, Jakhade AP, Kulkarni SD, Chikate RC. 1, 5 diphenyl carbazide immobilized cross-linked chitosan films: an integrated approach towards enhanced removal of Cr (VI). *J Mol Liq*. 2017;247:254–261. doi:10.1016/j.molliq.2017.09.122
32. El-Dakroury WA, El-Tokhy FS, Asaad GF, et al. Development, characterization, and optimization of folate-chitosan surface-modified PLGA-decorated mesoporous silica nanoparticles for effective delivery of leflunomide for the management of rheumatoid arthritis. *Eur J Pharm Biopharm*. 2025;214:114808. doi:10.1016/j.ejpb.2025.114808
33. Sallam AAM, Darwish SF, El-Dakroury WA, Radwan E. Olmesartan niosomes ameliorates the Indomethacin-induced gastric ulcer in rats: insights on MAPK and Nrf2/HO-1 signaling pathway. *Pharm Res*. 2021;38(11):1821–1838. doi:10.1007/S11095-021-03126-5/FIGURES/10
34. El-Dakroury WA, Zewail MB, Amin MM. Design, optimization, and in-vivo performance of glipizide-loaded O-carboxymethyl chitosan nanoparticles in insulin resistant/type 2 diabetic rat model. *J Drug Deliv Sci Technol*. 2023;79:104040. doi:10.1016/j.jddst.2022.104040
35. Bedi O, Krishan P. Investigations on acute oral toxicity studies of purpurin by application of OECD guideline 423 in rodents. *Naunyn Schmiedebergs Arch Pharmacol*. 2020;393(4):565–571. doi:10.1007/s00210-019-01742-y
36. Zewail MB, Nomier YA, Elesawy AE, El-Dakroury WA. Investigating the potential of quercetin-loaded chitosan-coated lipid carriers as an oral nanoplatform for depression management. *Int J Biol Macromol*.

37. Calvo–Torrent A, Brain PF, Martinez M. Effect of predatory stress on sucrose intake and behavior on the plus-maze in male mice. *Physiol Behav*. 1999;67(2):189–196. doi:10.1016/S0031-9384(99)00051-7
38. Belovicova K, Bogi E, Csatlosova K, Dubovicky M. Animal tests for anxiety-like and depression-like behavior in rats. *Interdiscip Toxicol*. 2017;10(1):40. doi:10.1515/intox-2017-0006
39. Ripoll N, Bronnec M, Bourin M. Nicotinic receptors and schizophrenia. *Curr Med Res Opin*. 2004;20(7):1057–1074. doi:10.1185/030079904125004060
40. Zewail MB, Asaad GF, Shabana ME, et al. PEGylated lipid polymeric nanoparticles for management of rheumatoid arthritis. *J Drug Deliv Sci Technol*. 2024;101(Part A):106242. doi:10.1016/j.jddst.2024.106242
41. Imran M, Iqubal MK, Imtiyaz K, et al. Topical nanostructured lipid carrier gel of quercetin and resveratrol: formulation, optimization, in vitro and ex vivo study for the treatment of skin cancer. *Int J Pharm*. 2020;587:119705. doi:10.1016/j.ijpharm.2020.119705
42. Agarwal S, Kumar SL, Garg R. Investigative study on impact of solid: liquid lipid ratio and stabilizer amount on some characteristics of nanostructure lipid carriers of quetiapine fumarate. *Int J Pharm Investig*. 2019;9(2):47–52. doi:10.5530/ijpi.2019.2.10
43. Chauhan I, Yasir M, Verma M, Singh AP. Nanostructured lipid carriers: a groundbreaking approach for transdermal drug delivery. *Adv Pharm Bull*. 2020;10(2):150. doi:10.34172/apb.2020.021
44. Kraisit P, Hirun N, Limpamanoch P, et al. Effect of Cremophor RH40, hydroxypropyl methylcellulose, and mixing speed on physicochemical properties of films containing nanostructured lipid carriers loaded with furosemide using the box–behnken design. *Polymers*. 2024;16(11):1605. doi:10.3390/polym16111605
45. Song A, Zhang X, Li Y, Mao X, Han F. Effect of liquid-to-solid lipid ratio on characterizations of flurbiprofen-loaded solid lipid nanoparticles (SLNs) and nanostructured lipid carriers (NLCs) for transdermal administration. *Drug Dev Ind Pharm*. 2016;42(8):1308–1314. doi:10.3109/03639045.2015.1132226
46. Saedi A, Rostamizadeh K, Parsa M, Dalali N, Ahmadi N. Preparation and characterization of nanostructured lipid carriers as drug delivery system: influence of liquid lipid types on loading and cytotoxicity. *Chem Phys Lipids*. 2018;216:65–72. doi:10.1016/j.chemphyslip.2018.09.007
47. Apostolou M, Assi S, Fatokun AA, Khan I. The effects of solid and liquid lipids on the physicochemical properties of nanostructured lipid carriers. *J Pharm Sci*. 2021;110(8):2859–2872. doi:10.1016/j.xphs.2021.04.012
48. Hendradi E, Rosita N, Rahmadhanniar E. Effect of lipid ratio of stearic acid and oleic acid on characteristics of nanostructure lipid carrier (NLC) system of diethylammonium diclofenac. *Indones J Pharm*. 2017;28(4):198–204. doi:10.14499/indonesianjpharm28iss4pp198
49. Kanwar R, Gradzielski M, Prevost S, et al. Effect of lipid chain length on nanostructured lipid carriers: comprehensive structural evaluation by scattering techniques. *J Colloid Interface Sci*. 2019;534:95–104. doi:10.1016/j.jcis.2018.08.066
50. Kristianingsih I, Hendradi E, Siswodihardjo S, Yuwono M. Development and physicochemical characterization of nanostructured lipid carriers for entrapment of vitamin D3 prepared at different lipid ratios. *Pharm Educ*. 2024;24(3):204–210. doi:10.46542/pe.2024.243.204210
51. Duong VA, Nguyen TTL, Maeng HJ. Preparation of solid lipid nanoparticles and nanostructured lipid carriers for drug delivery and the effects of preparation parameters of solvent injection method. *Molecules*. 2020;25(20):4781. doi:10.3390/molecules25204781
52. Lović J, Bogdanović A, Tadić V, et al. Electrochemical Behavior of Duloxetine hydrochloride at au and GC solid electrodes: its quantitative determination and degradation. *J Electrochem Soc*. 2022;169(7):76507. doi:10.1149/1945-7111/ac7e74
53. Said AR, Asaad GF, Shabana ME, et al. Desosomes and desimicelles− a novel vesicular and micellar system for enhanced oral delivery of poorly soluble drug: optimization of in vitro characteristics and in vivo performance. *Eur J Pharm Biopharm*. 2024;200:114324. doi:10.1016/j.ejpb.2024.114324
54. Peña-Juárez M, Palestino-Escobedo G, Navarrete-Damian J, et al. Water-mediated chelation dynamics of dicarboxylic acid functionalized TiO2 nanoparticles for β-nucleation enhancement in isotactic polypropylene composites. *Polym Technol Mater*. 2024;63(18):2549–2562.
55. Gonzalez-Calderon JA, Fierro-Gonzalez JC, Peña-Juarez MG, Perez E, Almendarez-Camarillo A. Influence of the chemical functionalization of titanium oxide nanotubes on the non-isothermal crystallization of polypropylene nanocomposites. *J Mater Sci*. 2022;57(10):5855–5872. doi:10.1007/s10853-022-07009-x
56. El-Dakroury WA, Zewail MB, Asaad GF, et al. Fexofenadine-loaded chitosan coated solid lipid nanoparticles (SLNs): a potential oral therapy for ulcerative colitis. *Eur J Pharm Biopharm*. doi:10.1016/j.ejpb.2024.114205
57. Pamlényi K, Kristó K, Sovány T, Regdon G Jr. Development and evaluation of bioadhesive buccal films based on sodium alginate for allergy therapy. *Heliyon*. 2022;8(8):e10364. doi:10.1016/j.heliyon.2022.e10364
58. Sattar M, Sayed OM, Lane ME. Oral transmucosal drug delivery–current status and future prospects. *Int J Pharm*. 2014;471(1–2):498–506. doi:10.1016/j.ijpharm.2014.05.043
59. Yuan G, Wang S, Gao W, Chen X. Effects of chitosan with different molecular weights on storage quality and fungi inhibition of mini-cucumber. *Food Control*. 2023;153:109905. doi:10.1016/j.foodcont.2023.109905
60. Román-Doval R, Torres-Arellanes SP, Tenorio-Barajas AY, Gómez-Sánchez A, Valencia-Lazcano AA. Chitosan: properties and its application in agriculture in context of molecular weight. *Polymers*. 2023;15(13):2867. doi:10.3390/polym15132867
61. Bravo-Osuna I, Vauthier C, Farabollini A, Palmieri GF, Ponchel G. Mucoadhesion mechanism of chitosan and thiolated chitosan-poly (isobutyl cyanoacrylate) core-shell nanoparticles. *Biomaterials*. 2007;28(13):2233–2243. doi:10.1016/j.biomaterials.2007.01.005
62. Moghaddam FA, Atyabi F, Dinarvand R. Preparation and in vitro evaluation of mucoadhesion and permeation enhancement of thiolated chitosan-pHEMA core-shell nanoparticles. *Nanomedicine Nanotechnol, Biol Med*. 2009;5(2):208–215. doi:10.1016/j.nano.2008.09.006
63. Mueller C, Verroken A, Iqbal J, Bernkop-Schnuerch A. Thiolated chitosans: in vitro comparison of mucoadhesive properties. *J Appl Polym Sci*. 2012;124(6):5046–5055. doi:10.1002/app.35622
64. Kurćubić I, Vajić UJ, Cvijić S, et al. Mucoadhesive buccal tablets with propranolol hydrochloride: formulation development and in vivo performances in experimental essential hypertension. *Int J Pharm*. 2021;610:121266. doi:10.1016/j.ijpharm.2021.121266
65. Koirala S, Nepal P, Ghimire G, et al. Formulation and evaluation of mucoadhesive buccal tablets of aceclofenac. *Heliyon*. 2021;7(3):e06439. doi:10.1016/j.heliyon.2021.e06439
66. Mansuri S, Kesharwani P, Jain K, Tekade RK, Jain NK. Mucoadhesion: a promising approach in drug delivery system. *React Funct Polym*. 2016;100:151–172.
67. Kumria R, Al-Dhubiab BE, Shah J, Nair AB. Formulation and evaluation of chitosan-based buccal bioadhesive films of zolmitriptan. *J Pharm Innov*. 2018;13:133–143. doi:10.1007/s12247-018-9312-6

68. Dinte E, Muntean DM, Andrei V, et al. In vitro and in vivo characterisation of a mucoadhesive buccal film loaded with doxycycline hyclate for topical application in periodontitis. *Pharmaceutics*. 2023;15(2):580. doi:10.3390/pharmaceutics15020580
69. Séquier F, Faivre V, Lanne JY, Daste G, Renouard M, Lesieur S. Critical steps during the prilling process of molten lipids: main stumbling blocks due to pharmaceutical excipient properties. *Int J Pharm*. 2020;576:119036. doi:10.1016/j.ijpharm.2020.119036
70. Matsaridou I, Barmpalexis P, Salis A, Nikolakakis I. The influence of surfactant HLB and oil/surfactant ratio on the formation and properties of self-emulsifying pellets and microemulsion reconstitution. *AAPS Pharm Sci Tech*. 2012;13:1319–1330. doi:10.1208/s12249-012-9855-7
71. Swain RP, Subudhi BB. Effect of Solutol HS 15 and Cremophor RH 40 on dissolution and bioavailability of nateglinide through solid dispersions. *Indian J Pharm Educ Res*. 2022;56(2):253–264. doi:10.5530/ijper.56.2s.96
72. Agarkhed M, O'Dell C, Hsieh MC, Zhang J, Goldstein J, Srivastava A. Effect of polysorbate 80 concentration on thermal and photostability of a monoclonal antibody. *AAPS Pharm Sci Tech*. 2013;14:1–9.
73. Pramod K, Suneesh CV, Shanavas S, Ansari SH, Ali J. Unveiling the compatibility of eugenol with formulation excipients by systematic drug-excipient compatibility studies. *J Anal Sci Technol*. 2015;6:1–14.
74. Micić D, Ostojić S, Pezo L, et al. Essential oils of coriander and sage: investigation of chemical profile, thermal properties and QSRR analysis. *Ind Crops Prod*. 2019;138:111438. doi:10.1016/j.indcrop.2019.06.001
75. Elsenosy FM, Abdelbary GA, Elshafeey AH, Elsayed I, Fares AR.Brain targeting of duloxetine HCL via intranasal delivery of loaded cubosomal gel: in vitro characterization, ex vivo permeation, and in vivo biodistribution studies. *Int J Nanomed*.2020;15:9517–9537. doi:10.2147/IJN.S277352
76. Mohd Amin USB, Osman NB, Uemura Y, NMNA M. Catalytic transfer hydrogenation of castor oil using glycerol-based reaction. *Waste Biomass Valorization*. 2020;11:5591–5597. doi:10.1007/s12649-020-01010-8
77. Madheswaran T, Baskaran R, Yong CS, Yoo BK. Enhanced topical delivery of finasteride using glyceryl monooleate-based liquid crystalline nanoparticles stabilized by cremophor surfactants. *AAPS Pharm Sci Tech*. 2014;15:44–51. doi:10.1208/s12249-013-0034-2
78. Gupta SA, Gaikwad AS, Mahajan AM. Tween-80 based ultra low-k (ULK) mesoporous films. *J Mater Sci Mater Electron*. 2017;28(19):14763–14768. doi:10.1007/s10854-017-7345-0
79. Barreiro-Iglesias R, Alvarez-Lorenzo C, Concheiro A. Thermal and FTIR Characterization of Films Obtained From Carbopol/Surfactant Aqueous Solutions. *J Therm Anal Calorim*. 2002;68(2):479–488. doi:10.1023/A:1016035618338
80. Gudi G, Krähmer A, Krüger H, Schulz H. Attenuated total reflectance–fourier transform infrared spectroscopy on intact dried leaves of sage (salvia officinalis l.): accelerated chemotaxonomic discrimination and analysis of essential oil composition. *J Agric Food Chem*. 2015;63(39):8743–8750. doi:10.1021/acs.jafc.5b03852
81. Khatoon M, Sohail MF, Shahnaz G, et al. Development and evaluation of optimized thiolated chitosan proniosomal gel containing duloxetine for intranasal delivery. *AAPS Pharm Sci Tech*. 2019;20:1–12. doi:10.1208/s12249-019-1484-y
82. Pereira GR, Collett JH, Garcia SB, Thomazini JA, Bentley MVLB. Glycerol monooleate/solvents systems for progesterone transdermal delivery: in vitro permeation and microscopic studies. *Rev Bras Ciências Farm*. 2002;38:55–62. doi:10.1590/S1516-93322002000100005
83. Acosta E. Bioavailability of nanoparticles in nutrient and nutraceutical delivery. *Curr Opin Colloid Interface Sci*. 2009;14(1):3–15. doi:10.1016/j.cocis.2008.01.002
84. Gunas V, Maievskyi O, Raksha N, et al. Study of the acute toxicity of scorpion leiurus macroctenus venom in rats. *Sci World J*. 2024;2024(1):9746092. doi:10.1155/2024/9746092
85. Choy EHS, Mease PJ, Kajdasz DK, et al. Safety and tolerability of duloxetine in the treatment of patients with fibromyalgia: pooled analysis of data from five clinical trials. *Clin Rheumatol*. 2009;28(9):1035–1044. doi:10.1007/s10067-009-1203-2
86. Rani R, Singh AP. Animals use to find anxiolytic activity: an updated review with advantage of each model. *J Drug Delivery Ther*. 2024;14(3).
87. David LK, Ibeachu PC, Hart JS. Assessment of anxiety and locomotive activity using elevated plus maze and open field tests in a Konzoinduced rat model. *EPRA Int J Multidiscip Res*. 2022;8(4):40–46.
88. Kruk-Slomka M, Dzik A, Biala G. The effects of indirect and direct modulation of endocannabinoid system function on anxiety-related behavior in mice assessed in the elevated plus maze test. *Molecules*. 2025;30(4):867. doi:10.3390/molecules30040867
89. Cryan JF, Holmes A. The ascent of mouse: advances in modelling human depression and anxiety. *Nat Rev Drug Discov*. 2005;4(9):775–790. doi:10.1038/nrd1825
90. Mohseni F, Rafaiee R. Opinion: ethical challenges in depression research: the tail suspension test, the forced swim test, and alternative behavioral models. *J Am Assoc Lab Anim Sci*. 2025;64(3):352–355. doi:10.30802/AALAS-JAALAS-24-131
91. Coppens E, Kempke S, Van Wambeke P, et al. Cortisol and subjective stress responses to acute psychosocial stress in fibromyalgia patients and control participants. *Psychosom Med*. 2018;80(3):317–326. doi:10.1097/PSY.0000000000000551
92. Yankelevitch-Yahav R, Franko M, Huly A, Doron R. The forced swim test as a model of depressive-like behavior. *J Vis Exp*. 2015;97:52587. doi:10.3791/52587
93. Carratalá-Ros C, Martínez-Verdú A, Olivares-García R, Salamone JD, Correa M. Effects of the dopamine depleting agent tetrabenazine in tests evaluating different components of depressive-like behavior in mice: sex-dependent response to antidepressant drugs with SERT and DAT blocker profiles. *Psychopharmacology*. 2023;240(8):1615–1628. doi:10.1007/s00213-023-06412-9
94. Carroll D, Ginty AT, Whittaker AC, Lovallo WR, De Rooij SR. The behavioural, cognitive, and neural corollaries of blunted cardiovascular and cortisol reactions to acute psychological stress. *Neurosci Biobehav Rev*. 2017;77:74–86. doi:10.1016/j.neubiorev.2017.02.025
95. Almutabagani LF, Almanqour RA, Alsabhan JF.Inflammation and treatment-resistant depression from clinical to animal study: a possible link? *Neurol Int*.2023;15:100–120. doi:10.3390/neurolint15010009
96. Dean J, Keshavan M. The neurobiology of depression: an integrated view. *Asian J Psychiatr*. 2017;27:101–111. doi:10.1016/j.ajp.2017.01.025
97. Qiu C, Yuan Z, He Z, et al. Lipopolysaccharide preparation derived from Porphyromonas gingivalis induces a weaker immuno-inflammatory response in BV-2 microglial cells than Escherichia coli by differentially activating TLR2/4-mediated NF-κB/STAT3 signaling pathways. *Front Cell Infect Microbiol*. 2021;11:606986. doi:10.3389/fcimb.2021.606986
98. Bymaster FP, Dreshfield-Ahmad LJ, Threlkeld PG, et al. Comparative affinity of duloxetine and venlafaxine for serotonin and norepinephrine transporters in vitro and in vivo, human serotonin receptor subtypes, and other neuronal receptors. *Neuropsychopharmacology*. 2001;25(6):871–880. doi:10.1016/S0893-133X(01)00298-6

99. Arora D, Bhatt S, Kumar M, Gautam RK, Taneja Y, Chauhan M. Significance of intranasal drug delivery systems: recent trends and clinical investigations in brain disorders. *Recent Adv Pharm Innov Res*. 447–477.
100. Paliwal R, SR P. *Nanomedicine, Nanotheranostics and Nanobiotechnology: Fundamentals and Applications*. CRC Press; 2025.
101. Camkurt MA, Fındıklı E, Bakacak M, Tolun Fİ, Karaaslan MF. Evaluation of malondialdehyde, superoxide dismutase and catalase activity in fetal cord blood of depressed mothers. *Clin Psychopharmacol Neurosci*. 2017;15(1):35. doi:10.9758/cpn.2017.15.1.35
102. Karakuş K, Demirci K, Uz E, Yiğit A, Özcankaya R. Effects of duloxetine on oxidant-antioxidant system in rat brain tissues. *Phoenix Med J*. 2024;6(1):16–21.
103. Saxena P, Selvaraj K, Khare SK, Chaudhary N. Superoxide dismutase as multipotent therapeutic antioxidant enzyme: role in human diseases. *Biotechnol Lett*. 2022;44(1):1–22. doi:10.1007/s10529-021-03200-3